Journal Pre-proof

ROS-Responsive and Multifunctional Anti-Alzheimer Prodrugs: Tacrine-Ibuprofen Hybrids via a Phenyl Boronate Linker

Zhikun Liu, Bin Zhang, Shengjin Xia, Lei Fang, Shaohua Gou

PII: S0223-5234(20)30969-7

DOI: https://doi.org/10.1016/j.ejmech.2020.112997

Reference: EJMECH 112997

To appear in: *European Journal of Medicinal Chemistry*

Received Date: 24 September 2020

Revised Date: 26 October 2020

Accepted Date: 3 November 2020

Please cite this article as: Z. Liu, B. Zhang, S. Xia, L. Fang, S. Gou, ROS-Responsive and Multifunctional Anti-Alzheimer Prodrugs: Tacrine-Ibuprofen Hybrids via a Phenyl Boronate Linker, *European Journal of Medicinal Chemistry*, https://doi.org/10.1016/j.ejmech.2020.112997.

Graphical abstract

ROS-Responsive and Multifunctional Anti-Alzheimer Prodrugs: Tacrine-Ibuprofen Hybrids via a Phenyl Boronate Linker

Zhikun Liu[a,b,1], Bin Zhang[a,b,1], Shengjin Xia[a,b], Lei Fang[a,b *], Shaohua Gou[a,b *]

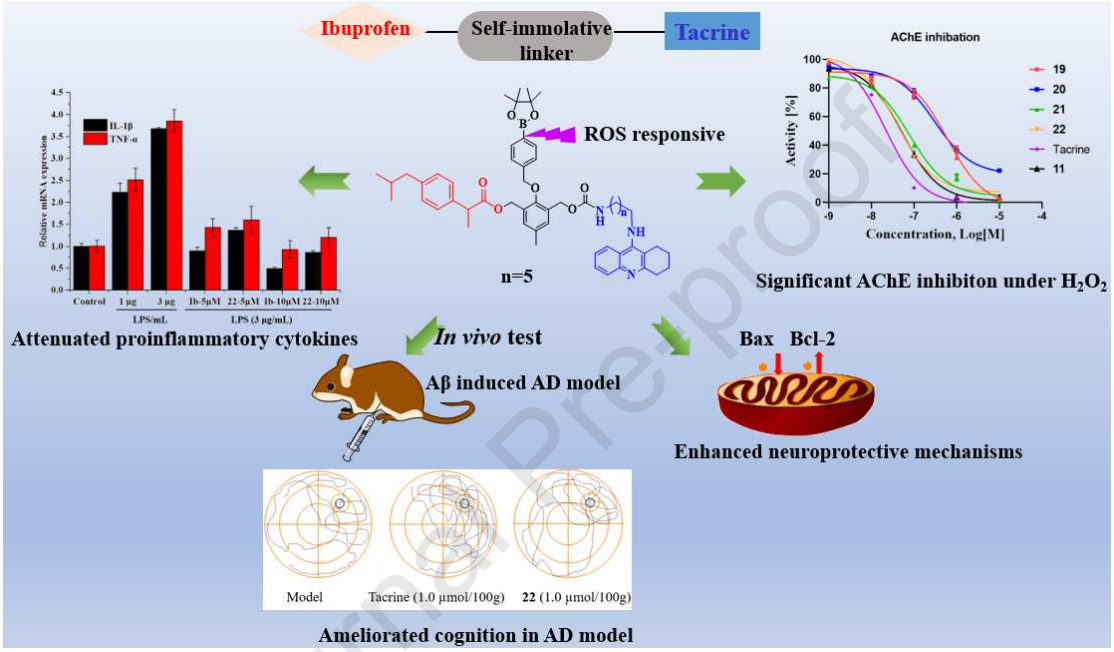

A series of ROS-responsive and multi-functional anti-Alzheimer compounds were designed and synthesized. The representative compound **22** possessed pronounced cholinesterase-inhibiting, anti-inflammatory and neuron-protective effects *in vitro*, and perfectly ameliorated the cognitive damage of AD *in vivo*. The study offers a promising strategy for developing new anti-Alzheimer drugs.

ROS-Responsive and Multifunctional Anti-Alzheimer Prodrugs: Tacrine-Ibuprofen Hybrids via a Phenyl Boronate Linker

Zhikun Liu [a,b,1], Bin Zhang[a,b,1],Shengjin Xia[a,b], Lei Fang[a,b *], Shaohua Gou[a,b *]

[a] *Jiangsu Province Hi-Tech Key Laboratory for Biomedical Research, Southeast University, Nanjing, 211189, China*

[b] *Pharmaceutical Research Center and School of Chemistry and Chemical Engineering, Southeast University, Nanjing 211189, China*

ABSTRACT Current drugs available in clinic for Alzheimer's disease (AD) treatment can only alleviate disease symptoms without clearly curing or delaying the process of AD. And some AD drugs failed in Phase III clinical trials are only focused on targeting amyloid-β (Aβ). Therefore, an alternative strategy in AD drug design is meaningful to be involved in the multiple pathogenic factors which can affect each other at multiple levels. Herein, we report a series of ROS-responsive prodrugs based on multi-target-directed ligands (MTDLs) approach, which can specifically release tacrine derivatives and ibuprofen under oxidation of ROS and show acetylcholinesterase (AChE)-inhibiting, neuron-protective and anti-inflammatory effects in extracellular or intracellular assays. Related biological study illustrated that compound **22** was able to permeate blood-brain-barrier (BBB) showing little hepatotoxicity in comparison to tacrine. Besides, **22** hinted a therapeutic clue in AD-treatment by regulating proinflammatory factors (IL-1β and TNF-α) and apoptosis related proteins (Bax, Bcl-2 and cleaved caspase-3). Further spatial memory assays in Aβ-induced AD model showed that **22** enhanced the ability of learning and memory. Our study proves that the strategy of ROS-responsive prodrugs has promise for AD treatments in future and offers a way for AD drug development.

---

[1]These authors contributed equally.

[*] Corresponding authors

E-mail: lei.fang@seu.edu.cn (L. Fang); 2219265800@qq.com (S. Gou)

Keywords: ROS stimulation, Prodrug, Multifunctional agent, Alzheimer

1. INTRODUCTION

Alzheimer's disease (AD), one of the most common forms of dementia, is an age-related neurodegenerative disease characterized by progressive cognitive decline, behavior disorders and degenerative brain disease [1,2]. It is estimated that about 50 million people have been affected by AD in 2018 and the number is expected to reach 152 million costing more than $2.0 trillion for treatment in the United States along by 2050 [3,4]. Without doubt, the sustaining and high-speed growth of AD patients will bring about huge social and economic burden, revealing that treatment of AD is of great significance.

Much attention has been paid to AD, but no efficient therapeutic treatment is developed at present because of complex etiology of this neurodegenerative disease and its multifactorial progression [5,6]. Several hypotheses based on AD's pathogenic factors have been proposed, including the production and aggregation of amyloid-β (Aβ), accumulation of hyperphosphorylated τ-proteins, oxidative stress, decrease of synaptic cholinergic level and inflammation response [7,8]. Upon these hypotheses, only a few of acetylcholinesterase inhibitors (AChEIs shown in **Figure 1**) including tacrine (withdrawn from the market for hepatotoxicity), donepezil, rivastigmine, galantamine and the N-methyl-D-aspartate receptor (NMDAR) antagonist (memantine), were obtained for AD treatment. However, these drugs can only alleviate the progress of AD by improving memory and cognitive function to a certain degree instead of definitively curing or stopping this disease. Therefore, development of novel approach to treat AD is much necessary and required. In view of the complex pathogenesis, present research and development on AD drugs are mainly focused on multitarget-directed ligands (MTDLs) approach by efficiently ameliorating memory and modifying cognitive decline [9-13].

Indeed, a number of drug candidates have undergone clinical trials and most of them aim to reduce the production of toxic aggregated Aβ or promote the depolymerization or clearance of aggregation Aβ proteins to protect neurons [14-17]. However, with further understanding of mechanisms about AD, oxidative stress is

found to happen earlier than other pathogenesis and then affect each other at multiple levels [18-20]. When dopamine (DA) is oxidized by oxygen (O_2) or upon the formation of metal ion-binding Aβ protein, a large number of reactive oxygen species (ROS) (e.g. superoxide anion radical ($O_2^{\bullet-}$) and hydrogen peroxide (H_2O_2) generate and subsequently induce more pathogenesis such as oxidative damage to biomolecules (lipids, proteins, and DNA), mitochondrial dysfunction and final disorders of neuronal homeostasis in the brain [21-23]. Moreover, prominent activation of inflammatory process (inflammatory cytokines, IL-1β, TNF-α) induced by Aβ may drive AD pathology or become ongoing disease process, though neuroinflammation exerts both toxic and protective effects in AD process [24-26]. Alternatively, in order to reduce the toxic side effects induced by anti-inflammatory drugs and increase neuron-protective activities, much attention has also been paid on microenvironment-responsive prodrug strategies [25, 27a].

In recent years, quite a number of H_2O_2-specific probes or H_2O_2-responsive prodrugs for antitumor study have been designed and synthesized using arylboronic acid or ester as the protecting group [27]. As a ROS-responsive unit, phenylboronate group can be self-immolative upon exposure to H_2O_2, which has been widely used in both oxidation-responsive polymers and prodrugs [28-30]. Tacrine, the first AChEI approved for AD treatment, has been withdrawn from clinical use, but we believe that it is still of great significance for further investigation on tacrine derivatives to reduce hepatotoxicity [6, 31,32]. Inkielewicz-Stepniak and co-workers have explained the great therapeutic potential of tacrine in Alzheimer's disease via multifunctional ligands modification [32c]. In addition, nonsteroidal anti-inflammatory drugs (NSAIDs) like ibuprofen or aspirin were reported to reduce inflammatory markers and reverse spatial memory deficits in APPsw transgenic mice or improve memory and learning, and decrease stress-related behaviors in FAD5X/Ppara-null mice [25,33,34]. Therefore, the great therapeutic potential effects of tacrine and ibuprofen motivate us to develop a novel agent to simultaneously tackle the cognitive impairment caused by Alzheimer's disease. Much different from 'one molecule, one target' paradigm, MTDLs approach usually offers more than one functional biological activities, which is suitable for

complex pathogenesis of AD. Besides, MTDLs approach can also offer an ample variety of derivatives in which key structure or linker length can modulate their biological properties. Moreover, considering the overproduction of ROS in brain of AD and specific characteristics of local inflammation, we have constructed self-immolative dendritic prodrugs consisting of two ligands, ibuprofen and tacrine derivatives, based on the MTDLs with a concept mentioned above.

As illustrated in **Figure 2**, we pursue to develop ROS-responsive prodrugs based on AD's pathological characteristics, including oxidative stress decreased synaptic cholinergic level and inflammation response. With this aim in mind, we expect these prodrugs release those two ligands at specific pathological oxidation environment of AD upon the stimulation of ROS. In order to achieve our designing goals, quite a number of biological assays have been performed including intracellular/extracellular tests and therapeutic effects in AD models in vivo. Herein we present such a promising strategy for the design of AD drugs as well as significant results we have obtained.

2. RESULTS AND DISCUSSION

2.1. Chemistry

Preparation of tacrine derivatives is shown in **Scheme S1**, in which intermediates **8**-**11** were synthesized according to the previous reports [31,32a]. Synthetic way of our target compounds **19**-**22** is displayed in **Scheme 1**. Compound **13** was obtained through modifying with two protection groups of TBDMS on **12**, using imidazole as an absorb acid agent in anhydrous N,N-dimethylformamide (DMF). Then, the nucleophilic substitution reaction between compound **13** and 4-bromomethylphenylboronic acid pinacol ester produced compound **14**. Intermediate **15** was obtained from deprotection reaction of **14** under the condition of catalytic amount of PTSA in methanol at room temperature. Single TBDMS-covered **16** was separated with silica gel chromatography. Compound **18** was made from deprotection of TBDMS-covered **17** followed by condensation reaction with ibuprofen. Compounds **19**-**22** were obtained by modifying two ligands of **18** and tacrine

derivatives **8**-**11**, respectively, in the presence of N,N'-carbonyldiimidazole (CDI) in DMF.

2.2. Cytotoxicity assay

Cytotoxicity of the target compounds (**19**-**22**) against SH-SY5Y cells was measured by MTT method. As shown in **Figure 3A**, no obvious cytotoxicity was induced by **19**-**22** in the concentration ranged from 7.81 to 31.25 μM. Interestingly, **19** (with a two-methylene linker) and **21** (with a four-methylene linker) exhibit moderate cytotoxicity to SH-SY5Y cells at 31.25 μM, whereas both of them have negligible cytotoxicity at 7.81 μM and 15.62 μM. Moreover, **20** (with a three-methylene linker) and **22** (with a six-methylene linker) have better cellular adaptability, especially for compound **22**. Judging from the results mentioned above, **22** exhibited negligible cytotoxicity to SH-SY5Y cells even at higher concentration of 31.25 μM as comparison to that of control group (**Figure 3A**), whereas **19**-**21** induced little to high cytotoxicity to some degree under this concentration. Therefore, we decided to select **22** to investigate the following biological activities in alleviating Alzheimer's disease.

As reducing the damage from oxidative stress in cells is believed to be feasible to protect the nerve cells [34b-34d], we subsequently investigated neuroprotective effects of compounds **19**-**22** against H_2O_2. Briefly, SH-SY5Y cells were pre-incubated with **19**-**22** followed by the addition of H_2O_2. After another 24 h co-incubation at 37 ^oC, cell viability of SH-SY5Y cells was obtained. The results in **Figure 3B** indicate that these compounds at the concentration of 5 μM show moderate to high neuroprotective activity against H_2O_2 and the values are all more than 50 % but significantly increase to more than 80 % when the concentration was elevated to 20 μM (exception for **21**), exerting stronger neuroprotective activities than that of H_2O_2-treated group (cell viability was about 20 %). However, ibuprofen, a component of the target compound, does not show apparent detoxification against H_2O_2. On the other hand, the combined group of ibuprofen and **11,** two components of **22**, seems not to rescue the cells against cytotoxicity induced by H_2O_2 even at high concentration of 20 μM. Taken all the results together, **22** is the most potential compound in protecting neurons. Thus, compound **22** is selected for further biological experiments.

Encouraged by this, we further investigate the H_2O_2-scavenging capability of our target compounds. The consuming H_2O_2 after 24 h co-incubation with **22** was quantified via QuantiChrom™ Peroxide Assay Kit. As illustrated in **Figure S1A,** the amount of scavenging H_2O_2 is significantly elevated in a liner relationship as the increasing dose of **22**. Trolox, a positive control, also shows strong H_2O_2-cosuming capacity (**Figure S1A)**. In contrast, **11** and ibuprofen only show negligible H_2O_2-eliminating capability as compared with **22** and Trolox. All the illustrated results mentioned above revealed that compound **22** can protect neurons from apoptosis against H_2O_2 and be beneficial for decrease of oxidation stress of Alzheimer.

*2.3. The release of ibuprofen and tacrine derivative **11***

The target compound, especially compound **22**, induces no cytotoxicity to SH-SY5Y cells (**Figure 3A**) but seems to be more potential in protecting neurons from apoptosis against the ROS (**Figure 3B**). Motivated by this, we evaluated the stability of compound **22** under the oxidation of H_2O_2. A mixed solution of **22** and H_2O_2 at 37 ^{o}C was used to detect the stability of **22** by reverse phase high performance liquid chromatography (RP-HPLC). For the purpose of matching the peaks generating from **22**, solutions of ibuprofen, **11** and **12** at certain concentrations were prepared. As shown in **Figure S1**, the peak attributed to **22** in RP-HPLC appeared at about 12.381 min (**Figure S1F**). However, when treated with H_2O_2, the peak of **22** gradually decreased with the generation of other three peaks matching the position of compound **11**, compound **12** and ibuprofen, respectively. This phenomenon indicated that **22** acted as a ROS-responsive prodrug. Moreover, the reaction rate did not accelerate a lot during the first 5 hours until the addition of another portion of H_2O_2, hinting that amount of H_2O_2 was scavenged with self-immolation of **22** (**Figure S1F**).

The results in **Figure S1F** indicated that **22** degrades into the fragments of **11**, **12** and ibuprofen gradually within 10 h upon stimulation with H_2O_2. Therefore, we speculated that the envisaged collapse mechanism of **22** under oxidative condition was as follows (**Scheme S3**): Firstly, phenylboronic ester reacted with H_2O_2 to

generate phenyl oxide structure. Subsequently, the electron rearrangement around the aromatic structure and finally caused rapidly release of the two ligands. In order to substantiate this speculation, the process was also monitored with ^{1}H-NMR characterization. As shown in **Figure S2**, initially, there existed no peaks from 4.10-4.60 ppm where were methylene protons of benzyl alcohols. However, when mixed with H_2O_2 (6.0 equiv.) at 37 ^oC, methylene protons of **22** (a, b) gradually decreased along with another increased peaks at 4.50 and 4.36 ppm (a′, b′, **Figure S2**). These two peaks (a′, b′) belong to the methylene protons of phenylboronate and cresol units, indicating the collapse of **22** under the oxidative condition of H_2O_2. Interestingly, the pinacol unmasking reaction was not detected may due to the fast degradation of this intermediate. Moreover, the significant changes in ^{1}H-NMR peaks of e′-f′ and c also proved the hydrolysis of the benzyl ester bonds and produce of fragments **11** and ibuprofen under the oxidative condition of H_2O_2. In sum, considering the results in **Figure S1F**, we can conclude that our target compound **22** served as a ROS-responsive prodrug and obtained great potential in treatment of Alzheimer's disease.

2.4. Blood-brain barrier (BBB) permeation and cellular uptake and assays

Brain permeation abilities are initially required for development of AD drugs [35a]. Therefore, in order to investigate the ability of **22** to penetrate the BBB we constructed a widely adopted BBB model by growing a dense layer of bEnd.3 cells on the upper chamber of a transwell [35b]. Briefly, bEnd.3 cells are cultured and allowed to adhere in monolayer in DMEM (10% FBS) and transendothelial electrical resistance (TEER) values of cells are monitored until the TEER values reach about 180 $\Omega \bullet cm^2$ and used for BBB assays. The schematic of BBB model is given in **Figure S3A** while change of TEER values during the monolayer culture is showed in **Figure S3B**. As illustrated in **Figure S3C**, TEER values are decreased in bEnd.3 cells monomers upon the addition of **22** while little change in TEER value occurs in DMSO-treated group. The decreased TEER at the first 15 min is induced by solvent, which was reported previously [36a]. Further immunofluorescence staining indicates that **22** induces discontinued intervals or even full absence to tight-junction related

protein (ZO-1) between bEnd.3 monomer cells (**Figure S3D**), which reveals that **22** regulates tight junction molecules to assist **22** to permeate BBB for delivering drug to brain. Furthermore, we also tested the content of **22** in the medium and intracellular abilities of lower chamber via BBB model by HPLC. As illustrated in **Figure S4B**, **22** easily passes through monomer cells in significant dose-dependent manner and can be easily ingested by SH-SY5Y cells in lower chamber (**Figure S4C**), indicating better BBB permeation abilities and intracellular properties. In sum, all of the results indicate that **22** efficiently permeates BBB via regulation expression of ZO-1 between bEnd.3 cells and easily entered SH-SY5Y cells.

For further research of visual experiment in BBB permeation assays and intracellular uptake assays, compound **25** with a fluorescent coumarin moiety at the position of **11** was constructed according to previous reports [36, 37] (**Scheme S2**). Intensely florescent images in SH-SY5Y cells in the BBB model indicate that **25** can efficiently cross through the monolayer barrier and be easily ingested by SH-SY5Y cells (**Figure S4D**). In order to investigate the uptake by SH-SY5Y and BV-2 cells, **25** were co-incubated with SY-SY5Y or BV-2 cells, respectively, and cellular uptake results were obtained from laser confocal microscope. The intensely florescent color in **Figure 4** indicates that **25** has entered either SY-SY5Y or BV-2 cells efficiently. Considering the great BBB permeation properties and efficient intracellular uptake of **22** and **25** in SHSY5Y cells we conclude that **22** is in great potential for treatment of Alzheimer's disease.

2.5. The AChE inhibition study

The results in **Figure S1F** illustrated that our target compounds act as ROS-responsive prodrugs upon stimulation with H_2O_2. Therefore, we forecast that AChE inhibition activity of our target compounds may vary greatly before and after treatment with H_2O_2. In order to confirm our hypothesis, AChE (from electric eel, eeAChE) inhibition assays were performed using tacrine and untreated-compounds **19**-**22** as controls with Ellman's methods [34, 38]. The decreased enzymatic activity results induced by **19**-**22** or H_2O_2-sitimulated **19**-**22** are shown in **Figure 5**. It is noted in **Figure 5A** that compounds **19**-**22** have moderate or no obvious AChE inhibitory

activity even at 10 μM. Besides, the inhibitory rate of AChE increased from 28.25% (**19**) to 47.25% (**22**), probably due to the extension of carbon linkers that enhanced the interaction between AChE and the tacrine group. However, after co-incubation with H_2O_2, the AChE inhibitory effects of the target compounds were enhanced apparently with the increasing alkyl chains. As shown in **Figure 5B**, H_2O_2-treated **19**-**22** exhibit AChE inhibitory activity with IC_{50} values in range of 39.16 - 608.1 nM, of which the activity of compound **22** containing a six methylene linker tacrine group is the strongest with a value comparable to that of tacrine (IC_{50} value was 21.63 nM) and **11** (IC_{50} value was 54.58 nM). It is noticed that the length of the alkyl chain has a close relationship with the AChE activity of the resulting compounds. Motivated by AChE inhibitory activity of **22**, we chose the compound **22** for the following biological study.

2.6. Molecular docking

The AChE inhibition study proved that our target compounds **19**-**22** showed little inhibitory effects on AChE, whereas they turned out to be efficient AChE imbibition agents upon exposure to H_2O_2. Generally, AChE was reported as dumbbell-shape with two active sites: the catalytic active site (CAS) at the bottom and the peripheral active site (PAS) at the lip [31]. To investigate the difference before and after treatment with H_2O_2, we performed the molecular docking studies of compounds **11** and **22**. The crystal structure of torpedo californica AChE (2CKM) was obtained from RSCB protein data bank, and the structure of **22** was constructed in Chem 3D 14.0 with energy minimized in Sybyl-X 2.0. The results obtained from Sybyl-X 2.0 surflex-dock model were shown in **Figure 6**. The binding model illustrated that the tacrine fragment of **11** bound to the bottom of AChE, is surrounded with Asp 72, Val 71, Tyr 70, Trp 84, Glu 199, Met 83, Gly 118 and Pro 86, exhibiting a potent π-π interaction between the heterocycle moiety and Trp 84; while the aliphatic alkyl chain is surrounded by Ser 200, Trp 84, Gly 441, His 440 and Try 442 (**Figure 6A** and **6B**). The formation of H-bond between aliphatic alkyl chain of **11** and residues Tyr 442 and Ser 200 may contribute to the inhibitory effect on AChE as well. However, the binding model in **Figure 6C** and **6D** suggested that **22** only occupies the mouth of the

gorge and was only surrounded with residues Gly 335, Phe 331, His 440, Asp 72, Val 71, Try 70, Asp 276 and Trp 279 without significant intermolecular interactions with residues around the PAS. Taken all these docking results together, the apparent difference of the binding models between **22** or **11** and AChE may explain why **22** shows little AChE inhibition activity excepting for stimulating with H_2O_2.

2.7. Inflammatory cytokines assay by qRT-PCR and LPS-induced ROS accumulation assays

Proinflammatory cytokines (such as TNF-α and IL-β) secreted by microglia play an important role in the pathogenesis and development of cognitive impairment [39-41]. Therefore, BV-2 cells were co-incubated with **22** for 6 h followed with treatment of LPS for another 24 h. The total RNA was isolated, purified, quantified and reversely transcripted to cDNA according to the previous report by q-PCR [25,39a]. The results in **Figure 7** showed that, under stimulation of LPS at concentration of 1 μg/mL and 3 μg/mL, expression of IL-1β was significantly increased to 2.22- and 3.68-fold, while that of TNF-α was significantly increased to 2.51- and 3.86-fold when compared to those of the control. This clearly indicates that LPS is capable of inducing inflammation in BV-2 cells. However, when co-incubated with **22** (5 μM, 10 μM) and LPS (3 μg/mL) for another 24 h, the expression of IL-1β in BV-2 cells decreased to 1.36- and 0.86-fold in a concentration-dependent manner while the expression of TNF-α decreased to 1.60- and 1.20-fold as comparison to control group (**Figure 7**). Moreover, the expression level of both IL-1β and TNF-α was decreased to the same level as that of untreated group, revealing that compound **22** acquired the anti-inflammatory activity by regulating relative proinflammatory cytokines (TNF-α and IL-β). Similarly, ibuprofen also showed the same anti-inflammatory effects by maintaining the normal level of the expression of TNF-α and IL-1β.

The results in **Figure 7** indicated that **22** modulates LPS-induced IL-1β and TNF-α to the normal levels in LPS-stimulated BV-2 cells as comparison with that of untreated cells, which may raise a question that whether the anti-inflammation effects come from **22** itself or from the released ibuprofen from **22** under the stimulation of LPS. No doubtfully, LPS elevated the intracellular ROS accumulation, which

thereafter modulates the expression of neurotoxic factors in microglia [39b]. Besides, disruption of the production or accumulation of intracellular ROS provides a method to investigate the proinflammatory signals in cells [39c]. Therefore, in order to investigate this mechanism of anti-inflammation of **22**, intracellular ROS accumulation in BV-2 cells were studied. As shown in **Figure S5**, the intracellular ROS levels in BV-2 cells treated with LPS (3 μg/mL) were significantly elevated (**Figure S5A2-S5C2**), labeling as more cells were stained in strong green-florescence as comparison with untreated-cells (**Figure S5A1-S5C1**). However, when co-incubated with **22** (10 μM) and LPS (3 μg/mL) for another 18 h, ROS levels were apparently decreased, illustrating that **22** regulated oxidative stress induced by LPS (**Figure S5A3-S5C3**). Interestingly, the remarkable ROS accumulation in the cells treated with combined group of ibuprofen (10 μM) and **11** (10 μM) indicated that both ibuprofen and **11** did not detoxify against LPS by eliminating the ROS accumulation (**Figure S5A4-S5C4**), though the cells were pretreated with the two components of **22** for 6 h. Moreover, BV-cells of 6 h pretreatment of LPS (3 μg/mL) and another 18 h co-incubation with **22** (10 μM) were also in normal ROS levels condition when compared with that of untreated cells (**Figure S5A5- S5C5**), revealing that **22** also showed neuroprotective activity in a model of oxidative stress in BV-2 cells. Taken the anti-inflammatory of **22** in LPS-treated cells in consideration, we believed that **22** rescued cells against cytotoxicity induced by LPS not only depending on the collapse of **22** in oxidative condition but also on its ROS-eliminating capability.

2.8. Apoptosis detection

On the basis of the promising neurons protection activity of **22** against H_2O_2, we subsequently performed apoptosis assays by FACS to investigate whether the neuroprotection was attributed to apoptosis inhibition. Firstly, the apoptosis of SH-SY5Y cells induced by **22** was studied. As shown in **Figure 8A-8D**, **22** did not exert obvious cytotoxicity against the cells after 24 h co-incubation with a cell viability value over 90%, consistent with the result observed in **Figure 3**. In order to evaluate the neuroprotective effect of **22** against H_2O_2, SH-SY5Y cells were incubated with **22** (5 μM, 10 μM) for 6 h followed by another 24 h treatment of H_2O_2 (100 μM).

Similarly, cells exposed to equal concentration H_2O_2 were used as positive control. The apoptotic results are given in **Figure 8E-8H**. Notably, the percentage of living cells decreased from 93.60% (DMSO-treated group) to 41.7% (H_2O_2-treated group). In comparison with H_2O_2, SH-SY5Y cells treated with **22** exhibited high percentage of living cells from 73.70% of **22** (5 μM) to 86.60% of **22** (10 μM). Significantly, the potency of **22** in protecting neurons from H_2O_2 induced cytotoxicity presented in a dose-dependent manner. In sum, these findings verify the results as obtained in **Figure 3** and the neuroprotective activity of compound **22**.

2.9. Hepatotoxicity study

Tacrine was the first AChEI approved for AD treatment, but it has been withdrawn from the clinical use due to its hepatotoxicity. However, this drug molecule still deserves to be investigated for non-hepatotoxic tacrine derivatives [31, 40-44]. It is learned that the hepatotoxicity induced by tacrine mainly resulted in elevating the levels liver transaminase, decreasing albumin concentration and inducing ROS in hepatocyte [31, 42-44]. In order to investigate whether our target compound can decrease the hepatotoxicity, compound **22** was used to for ROS accumulation tests with tacrine as positive control. As shown in **Figure 9**, in comparison to the control group, tacrine caused significant hepatotoxicity as illustrated with more HepG2 cells in green florescence. Interestingly, less amount of HepG2 cells in green florescence were detected when cells were treated with **22** (25 or 50 μM) for 24 h. Generally, the higher the accumulation of ROS was present, the more serious damage was induced to the cells [45,46]. Taken all of the results mentioned above, compound **22** caused lower hepatotoxicity at a concentration of 25 or 50 μM than tacrine which induced serious hepatotoxicity at 50 μM.

2.10. Cell morphology assays under H_2O_2

In order to investigate the change of cell morphology, calcein AM/PI double staining probes were used. SH-SY5Y cells were pre-incubated with **22** (10 μM) for 6 h at 37 ^{o}C, using DMSO as control group. Subsequently, the cells in **22**-treated group and untreated group were incubated with H_2O_2 (100 μM) for another 24 h and stained with calcein AM/PI double staining probes. As shown in **Figure 10**, the cells without

any treatment are in spindle outline and mostly stained in green florescence (**Figure 10A1**), while little cells are stained in red florescence (**Figure 10B1**). However, after treated with H_2O_2 most cells become oval or irregular nucleus in apoptosis or death state and are stained in red florescence by the PI probe (**Figure 10A2-10C2**). Moreover, after pre-treatment with **22** (**Figure 10B3**), less cells with red florescence are found as compared with H_2O_2-treated group (**Figure 10A2-10C2**), illustrating that **22** shows perfect neuroprotective activities against the apoptosis induced by H_2O_2. Besides, the neuroprotective effects also confirmed the better anti-apoptosis activity of **22** as evaluated in **Figure 8**.

2.11. Western blotting assays

Given the great potential neuroprotective activities of **22** revealed above, we subsequently explore the mechanism of its neuroprotective effects against cytotoxicity induced by H_2O_2 via western blotting technique. SH-SY5Y cells were pre-incubated with DMSO, **22**(5 μM, 10 μM), ibuprofen (10 μM) and ferulic acid (10 μM) for 6 h and subsequently treated with H_2O_2 (100 μM) for another 24 h. The total cytosolic protein of SH-SY5Y cells was collected and subjected to western blotting assay with β-actin as internal reference. As shown in **Figure 11**, levels of relative apoptosis related proteins of Bcl-2, Bax and cleaved-caspase 3 in H_2O_2-treated group are significantly changed in comparison to those of untreated-group, which clearly revealed that H_2O_2 can induce apoptosis through mitochondrial apoptosis pathway. However, when cells co-incubated with **22** and H_2O_2, the levels of Bax and cleaved-caspase 3 were decreased while Bcl-2 was up-regulated in contrast to those of H_2O_2-treated group, indicating that **22** exerted neural protective effects by regulating the expression of apoptotic protein and anti-apoptotic protein. Moreover, this neuroprotective ability of **22** was in a concentration-dependent manner in regulating related apoptotic proteins. As expected, the positive control (ferulic acid-treated cells) also exerted the same neuroprotective effects by regulating the expression of relative proteins.

2.12. Morris Water Maze (MWM) assay

Lastly, we carried out morris water maze (MWM) test to investigate the therapeutic effect of **22** on the learning and memory of AD model rats induced by intrahippocampal aggregated Aβ25-35 (2 μL, 5 μg/μL). After another a week recovery from the surgery, the rats were treated daily intraperitoneal injection of tacrine (1.0 μmol/100g b.wt., 0.2 mg/100g, qd), **22** (1.0 μmol/100g b.wt., 0.9 mg/100g, qd), using equal amount of normal saline for control group. As shown in **Figure 12**, the escape latency of rats in different groups had no significant difference of approximately 65 s. During the following four days, rats of tacrine-treated group and **22**-treated group displayed a significant decrease in escape latency, especially for short searching distance of tacrine-treated and **22**-treated groups on the day five (**Figure 12B**). Moreover, the shorter searching path of rats in **22**-treated group revealed that **22** gained better memory improvement than tacrine. Not surprisingly, the escape latency of the model group changed little in comparison to that of the first day. These results apparently proved that **22** can ameliorate cognitive deficit induced by Aβ polymers.

Furthermore, the results in **Figure 12C** indicated that rats in the control group swam aimlessly in the tank, whereas rats in tacrine-treated and **22**-treated groups preferentially swam in the northeast of the target quadrant. Similarly, rats in **22**-treated group took more time (2.2 seconds) in the targeting platform than that of the control or tacrine-treated rats (1.3 seconds), demonstrating that **22** has potential in ameliorating cognitive deficit and improving spatial memory when compared with tacrine-treated group. More excitingly, the more times (4.2) of **22**-treated rats crossed the platform than those of the control (0.4) and tacrine-treated rats (2.4) disclosed that **22** showed significantly therapeutic effect in ameliorating cognitive deficit and improving spatial memory of AD model rats.

3. CONCLUSION

In conclusion, a series of ROS-responsive prodrugs have been designed and synthesized based on the clinic pathological characteristics of ROS overproduction, inflammation and decrease of choline transmitters in brain. The prodrugs were constructed and catered to our design with MTDLs strategies as a potential and novel symptomatic- and disease-improving approach in AD treatments. The cytotoxicity

tests showed that the resulting compounds themselves had little cytotoxic activity toward SH-SY5Y cells, but exerted excellent neuron-protective effects in the presence of H_2O_2. Besides, little inhibitory activity on AChE was detected even at 10 μM, whereas H_2O_2-treated **19**-**22** showed AChE inhibitory activity with IC_{50} values from 39.16 to 608.1 nM. Further examination indicated that upon treatment with H_2O_2, **22** can release **11** and ibuprofen, and show strong neuroprotective by inhibiting proinflammatory cytokines (TNF-α and IL-1β) in LPS-treated microglial cells (BV-2) and regulating apoptosis related proteins (Bax, Bcl-2 and cleaved caspase-3). In addition, **22** showed neglected hepatotoxicity in HepG2 cells by inducing less intracellular ROS than tacrine, demonstrating that this compound has better biocompatibility. More importantly, compound **22** exhibited significantly therapeutic effect in ameliorating cognitive deficit and improving spatial memory of Aβ-induced AD model rats. Taken together, our research on these ROS-responsive prodrugs has promise for AD treatments in future and offers a way for developing new AD drugs.

4. EXPERIMENTAL SECTION

4.1. Materials and Instruments

All the reagents and solvents were reagent grade with a minimum purity of 98% purchased from Aladdin, Energy Chemical or Sinopharm Chemical Reagent Co., Ltd and were used without further purification. All reactions were carried out under nitrogen in anhydrous conditions, unless otherwise indicated. The ^{1}H-NMR and ^{13}C-NMR were recorded with Bruker 600 MHz spectrometer in DMSO-d_6 or $CDCl_3$ with TMS as the internal standard. Chemical shifts were obtained in parts per million (ppm) and spin multiplicities in NMR spectra were abbreviated as: s (singlet), d (doublet), t (triplet), m (multiplet) or br (broad). All of the intermediates and target products were purified by recrystallization or silica gel chromatography. Silica gel (200-300 mesh) was purchased from Qingdao Haiyang Chemical Co. Ltd. and was used without further treatment. Reactions were monitored by UV detector using thin player chromatography (TLC) on silica gel plates (Yantai Jiangyou Silica Gel Development Co., Ltd.). High-resolution mass spectrometry (HR-MS) were recorded by an Agilent 6224 ESI/TOF MS instrument. All target compounds with purity of

95% or above were used in the following biological studies. The purity testes were made with RP-HPLC (waters, e2695 system) equipped with ODS column (250×4.6 mm, 5 μm) and UV/Vis detector (2489 system, using wavelength of 254 nm), running 45:55 acetonitrile: water (V/V) (0.05% trifluoroacetic acid in water) at a flow rate of 1 mL/min. ROS tracker (KGAF018), mitochondrial membrane potential test kit (KGA604), and Annexin-V/PI double staining kit as well as the cells used were purchased from KeyGEN BioTECH Corp. Primary antibodies of Bax, Bcl-2 and cleaved capase-3 were obtained from Imgenex, USA. Secondary antibodies labeled with horseradish peroxidase with a dilution of 1:2000 were from Santa Cruz Biotechnologies. Primary antibody of anti-ZO-1 (ab216880) and secondary goat anti-rabbit IgG H&L (ab150077) were from Abcam. QuantiChrom™ Peroxide Assay Kit was purchased from BioAssay Systems, ROS tracker (DCFH-DA, S0033S, Beyotime).

4.2. Synthesis of Intermediates

*2,6-bis(((tert-butyldimethylsilyl)oxy)methyl)-4-methylphenol (**13**).* To a solution of compound **12** (4.0 g, 23.7 mmol) and imidazole (3.7 g, 54.5 mmol) in DMF (30 mL), TBDMSCl (7.9 g, 52.3 mmol) was added dropwise at 0 □and kept stirring for 2 h at the same temperature. After the completion of the reaction, EA (300 mL) was added to dissolve the residue. The resulting solution was washed with sat. saline solution three times. The organic layer was dried with anhydrous Na_2SO_4 and concentrated in vacuum to give crude oil, which was isolated on silica gel chromatography to give compound **13**. (colorless oil, 8.4 g). Yield 90.0%. ^{1}H NMR (600 MHz, $CDCl_3$) δ 8.03 (s, 1H, Ar-O<u>H</u>), 6.91 (s, 2H, Ar-<u>H</u>), 4.83 (s, 4H, Ar-C<u>H</u>$_2$), 2.26 (s, 3H, Ar-<u>H</u>), 0.95 (s, 18H, C(C<u>H</u>$_3$)$_3$), 0.13 (s, 12H, Si(C<u>H</u>$_3$)$_2$).

*(((5-methyl-2-((4-(4,4,5,5-tetramethyl-1,3,2-dioxaborolan-2-yl)benzyl)oxy)-1,3-phenylene)bis(methylene))bis(oxy))bis(tert-butyldimethylsilane) (**14**).* A solution of compound **13** (4.2 g, 10.6 mmol) in DMF (15 mL) was cooled to 0 °C, then K_2CO_3 (2.8 g, 20.2 mmol) was added and stirred for 10 min at the same temperature before the addition of 2-(4-bromobenzyl)-4,4,5,5-tetramethyl-1,3,2-dioxaborolane (3.0 g). After the completion of the reaction monitored by TLC, EA (300 mL) was added to

dissolve the residue that was washed with sat. saline solution three times. The organic layer was dried with anhydrous Na_2SO_4 and concentrated in vacuum to give crude colorless oil, which was purified by silica gel chromatography to obtain compound **14**. (colorless oil, 4.8 g). Yield 75.1%. ^{1}H NMR (600 MHz, $CDCl_3$) δ 7.85 (d, *J* = 8.0 Hz, 2H, Ar-H), 7.43 (d, *J* = 8.0 Hz, 2H, Ar-H), 7.18 (s, 2H, Ar-H), 4.90 (s, 2H, Ar-CH_2), 4.71 (s, 4H, Ar-CH_2), 2.35 (s, 3H, Ar-CH_3), 1.37 (s, 12H, OC(CH_3)$_2$), 0.93 (s, 18H, -C(CH_3)$_3$), 0.08 (s, 12H, -Si(CH_3)$_2$).

*(5-methyl-2-((4-(4,4,5,5-tetramethyl-1,3,2-dioxaborolan-2-yl)benzyl)oxy)-1,3-phenylene)dimethanol (**15**)*. To a solution of compound **14** (1.1 g, 1.86 mmol) in MeOH (15 mL) was added PTSA (35.4 mg). The mixture was stirred at room temperature for 30 min, then the solvent was removed under reduced pressure after the completion of the reaction. EA (150 mL) was added to dissolve the residue that was washed with sat. saline solution three times. The organic layer was dried with anhydrous Na_2SO_4 and concentrated in vacuum. The residue was isolated by silica gel chromatography to give compound **15** (colorless oil, 640.0 mg). Yield 89.5%. ^{1}H NMR (600 MHz, $CDCl_3$) δ 7.82 (d, *J* = 7.9 Hz, 2H, Ar-H), 7.40 (d, *J* = 7.9 Hz, 2H, Ar-H), 7.13 (s, 2H, Ar-H), 4.90 (s, 2H, Ar-CH_2), 4.62 (s, 4H, Ar-CH_2), 2.30 (s, 3H, Ar-CH_3), 1.35 (s, 12H, OC(CH_3)$_2$)).

*(3-(((tert-butyldimethylsilyl)oxy)methyl)-5-methyl-2-((4-(4,4,5,5-tetramethyl-1,3,2-dioxaborolan-2-yl)benzyl)oxy)phenyl)methanol (**16**)*. To a solution of compound **15** (1.5 g, 3.9 mmol) and imidazole (398.2 g, 5.9 mmol) in DMF (15 mL) was added TBDMSCl (764.0 g, 5.1 mmol) dropwise at 0 °C. The mixture was stirred overnight at room temperature. After the completion of the reaction monitored by TLC, EA (150 mL) was added to dissolve the residue that was washed with sat. saline solution three times. The organic layer was dried with anhydrous Na_2SO_4 and concentrated in vacuum to give crude oil, which was isolated on silica gel chromatography to obtain compound **16**. (colorless oil, 964.0 mg). Yield 49.6%. ^{1}H NMR (600 MHz, $CDCl_3$) δ 7.97 (s, 1H,), 7.85 (d, *J* = 7.9 Hz, 2H, Ar-H), 7.43 (d, *J* = 7.9 Hz, 2H, Ar-H), 7.22 (d, *J* = 1.5 Hz, 1H, Ar-H), 7.10 (d, *J* = 1.7 Hz, 1H, Ar-H), 4.93 (s, 2H, Ar-CH_2), 4.72 (s,

2H, Ar-C$\underline{H}_2$), 4.63 (s, 2H, Ar-C$\underline{H}_2$), 2.33 (s, 3H, Ar-C$\underline{H}_3$), 1.36 (s, 12H, -OC(C$\underline{H}_3$)$_2$), 0.93 (s, 9H, -C(C$\underline{H}_3$)$_3$), 0.09 (s, 6H, -Si(C$\underline{H}_3$)$_2$).

*3-(((tert-butyldimethylsilyl)oxy)methyl)-5-methyl-2-((4-(4,4,5,5-tetramethyl-1,3,2-dioxaborolan-2-yl)benzyl)oxy)benzyl 2-(4-isobutylphenyl)propanoate (**17**).* A solution of ibuprofen (1.48 g, 7.2 mmol) and DCC (1.9 g, 9.4 mmol) in anhydrous DCM (25 mL) was stirred at room temperature for 20 min. Then, compound **16** (3.2 g, 6.6 mmol) was added dropwise at the same temperature and stirred overnight. After the completion of the reaction, the deposit was filtered out and the organic layer was concentrated under reduced pressure. The residue was further isolated by silica gel chromatography with the eluent of PE and EA (30:1-25:1) to obtain compound **17**. (colorless oil, 3.4 g). Yield 75.6%. ^{1}H NMR (600 MHz, $CDCl_3$) δ 7.81 (d, *J* = 7.7 Hz, 2H, Ar-$\underline{H}$), 7.34 (d, *J* = 7.7 Hz, 2H, Ar-$\underline{H}$), 7.23 (s, 1H, Ar-$\underline{H}$), 7.17 (d, *J* = 8.0 Hz, 2H, Ar-$\underline{H}$), 7.04 (d, *J* = 8.0 Hz, 2H, Ar-$\underline{H}$), 6.93 (s, 1H, Ar-$\underline{H}$), 5.17-5.12 (m, 2H, Ar-C$\underline{H}_2$-O), 4.75 (s, 2H, Ar-C$\underline{H}_2$-O), 4.65 (s, 2H, Ar-C$\underline{H}_2$-O), 3.72 (q, *J* = 7.1 Hz, 1H, Ar-C$\underline{H}$-CO), 2.40 (d, *J* = 7.2 Hz, 2H, Ar-C$\underline{H}_2$-CH), 2.27 (s, 3H, Ar-C$\underline{H}_3$), 1.83-1.77 (m, 1H, -C$\underline{H}$(CH$_3$)$_2$), 1.49 (d, *J* = 7.2 Hz, 3H, CH(C$\underline{H}_3$)$_2$), 1.37 (s, 12H, -OC(C$\underline{H}_3$)$_2$), 0.92 (s, 9H, -C(C$\underline{H}_3$)$_3$), 0.88 (s, 3H, -CH(C$\underline{H}_3$)$_2$), 0.87 (s, 3H, -CH(C$\underline{H}_3$)$_2$), 0.06 (s, 6H, -Si(C$\underline{H}_3$)$_2$).

*3-(hydroxymethyl)-5-methyl-2-((4-(4,4,5,5-tetramethyl-1,3,2-dioxaborolan-2-yl) benzyl)oxy)benzyl 2-(4-isobutylphenyl)propanoate (**18**).* To a solution of compound **17** (3.7 g, 5.5 mmol) in MeOH (25 mL) PTSA (104.0 mg) was added. The mixture was stirred at room temperature for 30 min, the solvent was removed under reduced pressure and EA (150 mL) was added. The resulting solution was washed three times with sat. saline solution. The organic layer was dried with anhydrous Na_2SO_4 and concentrated in vacuum. The residue was isolated by silica gel chromatography to give compound **18**. (colorless oil, 1.9 g). Yield 63.0%. ^{1}H NMR (600 MHz, $CDCl_3$) δ 8.24 (d, *J* = 9.1 Hz, 2H, Ar-$\underline{H}$), 7.81 (d, *J* = 7.9 Hz, 2H, Ar-$\underline{H}$), 7.36 (d, *J* = 7.9 Hz, 2H, Ar-$\underline{H}$), 7.26 (d, *J* = 2.3 Hz, 1H, Ar-$\underline{H}$), 7.25 (d, *J* = 2.3 Hz, 1H, Ar-$\underline{H}$), 7.20 (d, *J* = 1.8 Hz, 1H, Ar-$\underline{H}$), 7.06 (d, *J* = 1.8 Hz, 1H, Ar-$\underline{H}$), 5.23 (s, 2H, Ar-C$\underline{H}_2$-O), 5.23 – 5.14 (m, 2H, Ar-C$\underline{H}_2$-O), 4.84 (s, 2H, Ar-C$\underline{H}_2$-O), 3.74 (q, *J* = 7.1 Hz, 1H,

Ar-C<u>H</u>-CO), 2.38 (d, *J* = 7.2 Hz, 2H, Ar-C<u>H</u>$_2$-CH), 2.27 (s, 3H, Ar-C<u>H</u>$_3$), 1.83 – 1.75 (m, 1H, -C<u>H</u>(CH$_3$)$_2$), 1.50 (d, *J* = 7.2 Hz, 3H, -CH(C<u>H</u>$_3$)), 1.36 (s, 12H, -OC(C<u>H</u>$_3$)$_2$), 0.87 (s, 3H, -CH(C<u>H</u>$_3$)$_2$), 0.86 (s, 3H, -CH(C<u>H</u>$_3$)$_2$).

*4.3. General preparations of compounds **19-22***

To a solution of compound **18** (300 mg, 0.52 mmol) in DMF (5 mL) CDI (92.8 mg, 0.57 mmol) was added. The mixture was stirred at room temperature for 2 h, then compound **8**/**9**/**10**/**11** (0.68 mmol) was added. After the resulting solution was kept stirring for another 2 h, DCM (150 mL) was added. The organic phase was washed three times with sat. saline solution, and then dried over anhydrous Na_2SO_4 and concentrated in vacuum. The residue was isolated by silica gel chromatography with the eluent of DCM and MeOH (40:1-10:1) to generate target compounds **19**-**22**.

*5-methyl-3-((((2-((1,2,3,4-tetrahydroacridin-9-yl)amino)ethyl)carbamoyl)oxy)methyl)-2-((4-(4,4,5,5-tetramethyl-1,3,2-dioxaborolan-2-yl)benzyl)oxy)benzyl2-(4-isobutylphenyl)propanoate (**19**)*. (pale yellow solid, 150 mg). Yield 34.3 %. ^{1}H NMR (600 MHz, $CDCl_3$) δ 14.40 (s, 1H, -N<u>H</u>-), 8.23 (d, *J* = 8.5 Hz, 1H, Ar-<u>H</u>), 8.11 (d, *J* = 8.5 Hz, 1H, Ar-<u>H</u>), 7.76 (d, *J* = 7.9 Hz, 2H, Ar-<u>H</u>), 7.35 (d, *J* = 7.9 Hz, 2H, Ar-<u>H</u>), 7.20 – 7.15 (m, 2H, Ar-<u>H</u>), 7.14 (d, *J* = 8.0 Hz, 2H, Ar-<u>H</u>), 7.02 (d, *J* = 8.0 Hz, 3H, Ar-<u>H</u>), 6.94 (s, 1H, Ar-<u>H</u>), 6.64 (s, 1H, -N<u>H</u>-), 5.15 (s, 2H, Ar-C<u>H</u>$_2$-O), 5.15 – 5.08 (m, 2H, Ar-C<u>H</u>$_2$-O), 4.80 (s, 2H, Ar-C<u>H</u>$_2$-O), 4.07 (s, 2H, NHC<u>H</u>$_2$-), 3.71-3.67 (m, 3H, Ar-C<u>H</u>-CO, NHC<u>H</u>$_2$-), 3.15 (s, 2H, -C<u>H</u>$_2$-), 2.45 (s, 2H, -C<u>H</u>$_2$-), 2.38 (d, *J* = 7.2 Hz, 2H, Ar-C<u>H</u>$_2$-CH), 2.19 (s, 3H, Ar-C<u>H</u>$_3$), 1.81-1.73 (m, 5H, -C<u>H</u>(CH$_3$)$_2$, -C<u>H</u>$_2$-), 1.46 (d, *J* = 7.2 Hz, 3H, -CH(C<u>H</u>$_3$)), 1.33 (s, 12H, -OC(C<u>H</u>$_3$)$_2$), 0.86 (s, 3H, -CH(C<u>H</u>$_3$)$_2$), 0.85 (s, 3H, -CH(C<u>H</u>$_3$)$_2$); ^{13}C NMR (150 MHz, $CDCl_3$) δ 174.44, 158.65, 155.54, 153.10, 150.65, 140.62, 139.88, 138.28, 137.41, 134.96(C×2，<u>Ar</u>-H，overlapped signals), 134.20, 131.72, 130.87, 130.61, 129.51, 129.47, 129.40, 129.34(C×2，<u>Ar</u>-H，overlapped signals), 127.19(C×2，<u>Ar</u>-H，overlapped signals), 126.89(C×2, <u>Ar</u>-H，overlapped signals), 124.69, 124.40, 120.04, 115.42, 110.91, 83.87(C×2 ，CH$_3$-<u>C</u>-(CH$_3$)$_2$, overlapped signals), 62.21, 61.51, 50.66, 45.12, 44.97, 40.71, 30.13,

29.70, 28.33, 24.88(C×4, -$\underline{CH}_3$,overlapped signals), 23.87, 22.39, 21.87, 20.79, 20.60, 18.35, 14.11； HR-MS(ESI) calcd for $[M+H]^+$ = 840.4759, found 840.4827.

5-methyl-3-((((3-((1,2,3,4-tetrahydroacridin-9-yl)amino)propyl)carbamoyl)oxy) methyl)-2-((4-(4,4,5,5-tetramethyl-1,3,2-dioxaborolan-2-yl)benzyl)oxy)benzyl2-(4-iso butylphenyl)propanoate (**20**). (pale yellow solid, 134.4 mg). Yield 30.3 %. ^{1}H NMR (600 MHz, CDCl3) δ 14.69 (s, 1H, -N$\underline{H}$-), 8.45 (d, J = 8.5 Hz, 1H, Ar-$\underline{H}$), 8.16 (d, J = 8.5 Hz, 1H, Ar-$\underline{H}$), 7.77 (d, J = 7.8 Hz, 2H, Ar-$\underline{H}$), 7.61 (t, J = 7.8 Hz, 1H, Ar-$\underline{H}$), 7.38 (t, J = 7.8 Hz, 1H, Ar-$\underline{H}$), 7.34 (d, J = 7.7 Hz, 2H, Ar-$\underline{H}$), 7.32 (s, 1H, Ar-$\underline{H}$), 7.15 (d, J = 7.9 Hz, 2H, Ar-$\underline{H}$), 7.03 (d, J = 7.9 Hz, 2H, Ar-$\underline{H}$), 6.94 (s, 1H, Ar-$\underline{H}$), 5.78 (s, 1H, -N$\underline{H}$-), 5.16 – 5.09 (m, 4H, Ar-C$\underline{H}_2$-O), 4.79 (s, 2H, Ar-C$\underline{H}_2$-O), 3.88 (s, 2H, NHC$\underline{H}_2$-), 3.72-3.68 (m, 1H, Ar-C$\underline{H}$-CO), 3.37-3.34 (m, 2H, -NHC$\underline{H}_2$-), 3.27-3.24 (m, 2H, -C$\underline{H}_2$-), 2.66 (s, 2H, -CH_2-), 2.38 (d, J = 7.2 Hz, 2H, Ar-C$\underline{H}_2$-CH), 2.20 (s, 3H, Ar-C$\underline{H}_3$), 1.84-1.76 (m, 7H, -C$\underline{H}$(CH_3)$_2$, -C$\underline{H}_2$-), 1.47 (d, J = 7.1 Hz, 3H, -CH(C$\underline{H}_3$)), 1.32 (s, 12H, -OC(C$\underline{H}_3$)$_2$), 0.86 (s, 3H, -CH(C$\underline{H}_3$)$_2$), 0.85 (s, 3H, -CH(C$\underline{H}_3$)$_2$); ^{13}C NMR (150 MHz, $CDCl_3$) δ 174.46, 157.75, 155.80, 153.29, 151.17, 140.62, 139.97, 138.61, 137.45, 134.97(C×2，$\underline{Ar}$-H, overlapped signals), 134.08, 132.14, 130.80, 130.79, 129.61, 129.42, 129.38, 129.35(C×2，$\underline{Ar}$-H, overlapped signals), 127.21(C×2，$\underline{Ar}$-H, overlapped signals), 126.89(C×2，$\underline{Ar}$-H, overlapped signals), 125.21, 123.93, 120.79, 115.76, 111.29, 83.86(C×2, CH_3-$\underline{C}$-(CH_3)$_2$, overlapped signals), 62.13, 61.54, 45.15, 44.98, 43.70, 37.28, 31.24, 30.13, 28.46, 24.87(C×4, -$\underline{C}H_3$, overlapped signals), 24.17, 22.39, 22.38, 22.04, 20.79, 20.66, 18.37, 14.13; HR-MS(ESI) calcd for $[M+H]^+$ = 854.4916, found 854.5190.

5-methyl-3-((((4-((1,2,3,4-tetrahydroacridin-9-yl)amino)butyl)carbamoyl)oxy)me thyl)-2-((4-(4,4,5,5-tetramethyl-1,3,2-dioxaborolan-2-yl)benzyl)oxy)benzyl2-(4-isobut ylphenyl)propanoate (**21**). (pale yellow solid, 141.0 mg). Yield 31.2 %. ^{1}H NMR (600 MHz, DMSO) δ 13.89 (s, 1H, -N$\underline{H}$-), 8.37 (d, *J* = 8.5 Hz, 1H, Ar-$\underline{H}$), 7.94 (d, *J* = 8.5 Hz, 1H, Ar-$\underline{H}$), 7.83 (t, *J* = 7.7 Hz, 1H, Ar-$\underline{H}$), 7.73 (s, 1H, Ar-$\underline{H}$), 7.66 (d, *J* = 7.8 Hz, 2H, Ar-$\underline{H}$), 7.54 (t, *J* = 7.7 Hz, 1H, Ar-$\underline{H}$), 7.35 (d, *J* = 7.8 Hz, 2H, Ar-$\underline{H}$), 7.28 (t, *J* = 5.6 Hz, 1H, Ar-$\underline{H}$), 7.14 (d, *J* = 8.1 Hz, 2H, Ar-$\underline{H}$), 7.04 (d, *J* = 8.0 Hz, 2H, Ar-$\underline{H}$), 6.92 (s, 1H, -N$\underline{H}$-), 5.09 (d, *J* = 12.6 Hz, 1H, Ar-C$\underline{H}_2$-O), 5.04 (d, *J* = 12.5 Hz, 1H,

Ar-C$\underline{H}_2$-O), 4.97 (s, 2H, Ar-C$\underline{H}_2$-O), 4.76 (s, 2H, Ar-C$\underline{H}_2$-O), 3.84-3.82 (m, 2H, NHC$\underline{H}_2$-), 3.79 – 3.75 (m, 1H, Ar-C$\underline{H}$-CO), 3.01-2.98 (m, 4H, -NHC$\underline{H}_2$-, -CH_2-), 2.64 (s, 2H, -CH_2-), 2.35 (d, *J* = 7.1 Hz, 2H, Ar-C$\underline{H}_2$-CH), 2.16 (s, 3H, Ar-C$\underline{H}_3$), 1.81-1.80 (m, 4H, -CH_2), 1.77-1.68 (m, 3H, -C$\underline{H}_2$-), 1.47 – 1.43 (m, 2H, -C$\underline{H}_2$-), 1.36 (d, *J* = 7.1 Hz, 3H, -CH(C$\underline{H}_3$)), 1.30 (s, 12H, -OC(C$\underline{H}_3$)$_2$), 0.81 (s, 3H, -CH(C$\underline{H}_3$)$_2$), 0.81 (s, 3H, -CH(C$\underline{H}_3$)$_2$). ^{13}C NMR (150 MHz, $CDCl_3$) δ 174.48, 156.62, 155.50, 153.22, 151.17, 140.62, 139.92, 138.67, 137.43, 134.97(C×2，Ar-H, overlapped signals), 134.06, 132.20, 130.79, 130.68, 129.77, 129.34(C×3，Ar-H, overlapped signals), 127.20(C×3，Ar-H, overlapped signals), 127.00(C×2，Ar-H, overlapped signals), 125.12, 124.30, 120.71, 115.72, 110.84, 83.86(C×2, CH_3-C-$(CH_3)_2$, overlapped signals), 61.70, 61.55(C×2, Ar-C$\underline{H}_2$-O, overlapped signals), 45.14, 44.97, 40.20, 31.58, 30.13, 28.37, 27.96, 27.04, 24.87(C×4, -C$\underline{H}_3$, overlapped signals), 22.38(C×2,-C$\underline{H}_2$-, overlapped signals), 21.89, 20.79, 20.59, 18.35, 14.14; HR-MS(ESI) calcd for $[M+H]^+$ = 868.5072, found 868.5058.

*5-methyl-3-((((6-((1,2,3,4-tetrahydroacridin-9-yl)amino)hexyl)carbamoyl)oxy)methyl)-2-((4-(4,4,5,5-tetramethyl-1,3,2-dioxaborolan-2-yl)benzyl)oxy)benzyl2-(4-isobutylphenyl)propanoate (**22**)*. (pale yellow solid, 116.4 mg). Yield 25.0 %. ^{1}H NMR (600 MHz, $CDCl_3$) δ 15.10 (s, 1H, -N$\underline{H}$-), 8.53 (d, *J* = 8.5 Hz, 1H, Ar-$\underline{H}$), 8.18 (d, *J* = 8.5 Hz, 1H, Ar-$\underline{H}$), 7.78 (d, *J* = 7.7 Hz, 2H, Ar-$\underline{H}$), 7.66 (t, *J* = 7.7 Hz, 1H, Ar-$\underline{H}$), 7.41 (t, *J* = 7.7 Hz, 1H, Ar-$\underline{H}$), 7.33 (d, *J* = 7.7 Hz, 2H, Ar-$\underline{H}$), 7.14 (d, *J* = 7.9 Hz, 2H, Ar-$\underline{H}$), 7.12 (s, 1H, Ar-$\underline{H}$), 7.03 (d, *J* = 7.9 Hz, 2H, Ar-$\underline{H}$), 6.94 (s, 1H, Ar-$\underline{H}$), 5.99 (s, 1H, -NH-), 5.16 – 5.05 (m, 4H, Ar-C$\underline{H}_2$-O), 4.89 (t, *J* = 5.7 Hz, 1H, NH-C$\underline{H}_2$), 4.77 (s, 2H, Ar-C$\underline{H}_2$-O), 3.90-3.87 (m, 2H, -NH-C$\underline{H}_2$-), 3.70 (q, *J* = 7.1 Hz, 1H, Ar-C$\underline{H}$-CO), 3.29 (t, *J* = 6.1 Hz, 2H), 3.19-3.15 (m, 2H, -CH_2-), 2.58 (t, *J* = 5.8 Hz, 2H, -CH_2-), 2.38 (d, *J* = 7.2 Hz, 2H, Ar-C$\underline{H}_2$-CH), 2.21 (s, 3H, Ar-C$\underline{H}_3$), 1.80-1.80 (m, 2H, -C$\underline{H}_2$-), 1.84 – 1.77 (m, 6H, -C$\underline{H}_2$-), 1.47-1.46 (m, *J* = 7.2 Hz, 7H, -C$\underline{H}_2$-), 1.34 (s, 12H, -OC(C$\underline{H}_3$)$_2$), 0.86 (s, 3H, -CH(C$\underline{H}_3$)$_2$), 0.85 (s, 3H, -CH(C$\underline{H}_3$)$_2$); ^{13}C NMR (150 MHz, $CDCl_3$) δ 174.44, 156.48, 155.46, 153.38, 151.30, 140.60, 139.94, 138.85, 137.47, 134.98(C×2，Ar-H), 134.05, 132.24, 130.97, 130.81, 129.79(C×2，Ar-H), 129.40,

129.34(C×2，Ar-H), 127.21(C×2，Ar-H), 126.98(C×2，Ar-H), 125.12, 124.27, 120.95, 115.78, 110.74, 83.85(C×2, CH_3-C-(CH_3)$_2$, overlapped signals), 61.73, 61.58(C×2, Ar-CH_2-O-, overlapped signals), 45.15, 44.99, 40.59, 30.91, 30.12, 29.81, 28.38, 26.03, 26.00, 24.88(C×4,-CH_3,), 23.80, 22.40, 22.38, 21.93, 20.78, 20.65, 18.37, 14.13; HR-MS(ESI) calcd for $[M+H]^+$ = 896.5585, found 896.5562.

*6-((2-oxo-2H-chromen-7-yl)oxy)hexanoic acid (**24**).* To a solution of compound **23** (1.0 g, 6.17 mmol) in DMF (10 mL), K_2CO_3 (3.4 g, 24.8 mmol), 6-bromohexanoic acid (2.4 g, 12.34 mmol) and catalytic amount of KI were added. The resulting solution was stirred at 55 ^oC for 6 h, then the solvent was removed under reduced pressure. The residue was isolated on silica gel with the eluent of DCM and MeOH (80:1-50:1) to produce compound **24**. Pale yellow solid (1.3 g). Yield 76.5%. ^1H NMR (600 MHz, DMSO) δ 12.00 (s, 1H, -COOH), 7.98 (d, *J* = 9.5 Hz, 1H, Ar-H), 7.61 (d, *J* = 8.6 Hz, 1H, Ar-H), 6.97 (d, *J* = 2.4 Hz, 1H, Ar-H), 6.93 (dd, *J* = 8.6, 2.4 Hz, 1H, Ar-H), 6.27 (d, *J* = 9.5 Hz, 1H, Ar-H), 4.06 (t, *J* = 6.5 Hz, 2H, Ar-O-CH_2-), 2.23 (t, *J* = 7.4 Hz, 2H, -CH_2-COOH), 1.76 – 1.71 (m, 2H, -CH_2-), 1.6-1.54 (m, 2H, -CH_2-), 1.45-1.39 (m, 2H, -CH_2-).

*3-(((2-(4-isobutylphenyl)propanoyl)oxy)methyl)-5-methyl-2-((4-(4,4,5,5-tetramethyl-1,3,2-dioxaborolan-2-yl)benzyl)oxy)benzyl6-((2-oxo-2H-chromen-7-yl)oxy)hexanoate (**25**).* DCC (174.5 g, 0.84 mmol) was added to a solution of compound **24** (180.0 mg, 0.65 mmol) in DCM (15 mL). The mixing solution was stirred for 10 min until white solids precipitated. Then, compound **17** (372.1 mg, 0.65 mmol) and catalytic amount of DMAP was added to the solution which was stirred for another 2 h. After removal of the precipitate, the product was isolated with silica gel chromatography with the eluent of EA and PE (10:1-5:1) as compound **25** (150 mg, white solid). Yield 27.8 %. ^1H NMR (600 MHz, $CDCl_3$) δ 7.80 (d, *J* = 8.0 Hz, 2H, Ar-H), 7.62 (d, *J* = 3.9 Hz, 1H, Ar-H), 7.35 – 7.34 (m, 3H, Ar-H), 7.16 (d, *J* = 8.0 Hz, 2H, Ar-H), 7.13 (d, *J* = 1.9 Hz, 1H, Ar-H), 7.04 (d, *J* = 8.0 Hz, 2H, Ar-H), 6.98 (d, *J* = 1.9 Hz, 1H, Ar-H), 6.81-6.79 (m, 1H, Ar-H), 6.78 (d, *J* = 2.3 Hz, 1H, Ar-H), 6.24 (d, *J* = 9.4 Hz, 1H, Ar-H), 5.17 – 5.11 (m, 2H, Ar-CH_2-O), 5.11 (s, 2H, Ar-CH_2-O), 4.80 (s, 2H, Ar-CH_2-O), 3.97 (t, *J* = 6.4 Hz, 2H, -O-CH_2-), 3.71 (q, *J* = 7.1 Hz, 1H, Ar-CH(CH_3)),

2.40 (d, *J* = 7.2 Hz, 2H, Ar-C$\underline{H}_2$-CH(CH_3)$_2$), 2.34 (t, *J* = 7.5 Hz, 2H, OOCC$\underline{H}_2$), 2.24 (s, 3H, Ar-C$\underline{H}_3$-), 1.83-1.76 (m, 3H, -C$\underline{H}_2$-, -C$\underline{H}$(CH_3)$_2$), 1.71-1.66 (m, 2H, -C$\underline{H}_2$-), 1.51 – 1.46 (m, 5H, -CH_2-, Ar-CH(C$\underline{H}_3$)), 1.35 (s, 12H, -OC(C$\underline{H}_3$)$_2$), 0.87 (d, *J* = 0.9 Hz, 3H, -CH(C$\underline{H}_3$)$_2$), 0.86 (d, *J* = 0.9 Hz, 3H, -CH(C$\underline{H}_3$)$_2$). ^{13}C NMR (150 MHz, $CDCl_3$) δ 174.45, 173.26, 162.31, 161.32, 155.91, 153.72, 143.48, 140.61, 139.95, 137.52, 135.03(C×2, Ar-H, overlapped signals), 134.11, 131.29, 131.16, 129.53, 129.36(C×2, Ar-H, overlapped signals), 129.27, 128.74(C×2, Ar-H, overlapped signals), 127.24(C×2, Ar-H, overlapped signals), 126.88(C×2, Ar-H, overlapped signals), 112.98, 112.94, 112.45, 101.37, 83.86(C×2, CH3-C(CH_3)$_2$, overlapped signals), 76.99, 68.28, 61.63, 61.51, 45.19, 45.01, 34.13, 30.15, 28.67, 25.57, 24.90(C×4, -CH_3, overlapped signals), 24.58, 22.42, 22.40, 20.78, 18.39.

4.4. Cell Culture

SH-SY5Y, BV-2, and b.End.3 cells were maintained in RPMI 1640 or Dulbecco's Modified Eagle Medium (DMEM, Life Technologies) supplemented with 10 % fetal bovine serum (FBS, Gibco), penicillin (100 U/mL) and streptomycin (100 μg/mL) solution. All cells were grown at 37 °C in 5% CO_2 atmosphere and 95% air.

4.5. Cytotoxicity assay

The cytotoxicity was measured with MTT methods. SH-SY5Y cells were seeded into 96-well plates at a density of 1×10^5 cells/mL and allowed to adhere for overnight. Then compounds of **19**-**22** and tacrine at different concentrations in DMSO were added to the well and co-incubated for 24 h, 48 h or 72 h at an atmosphere of 5 % CO_2 and 95 % air. Subsequently, MTT (5 mg/mL) was added for an extra 4 h of incubation. The medium was replaced with DMSO to dissolve formazan precipitate and the absorbance of OD was recorded with enzyme-labeling instrument at a wavelength of 570 nm. The results of cell viabilities were analyzed with SPSS software for three independent experiments. Neuroprotective assays of **19**-**22** were carried out followed the procedures mentioned above. Briefly, SH-SY5Y cells were pre-incubated with **19**-**22** (5, 10, 20 μM), ibuprofen (5, 10, 20 μM) and combined group (ibuprofen and **11**, 5, 10, 20 μM) for 6 h followed with another 24h treatment of

H_2O_2. The results obtained through MTT assays were shown as mean ± SD of three independent experiments.

*4.6. Release of ibuprofen and tacrine derivative **11***

A solution of **22** (40 μmmol/L) was prepared in purified water and acetonitrile (50 % : 50 %, V/V), then the solution of **22** and H_2O_2 (3.0 equiv.) were co-incubated at 37 ^oC in dark. The release process was recorded and analyzed with reversed phase high performance liquid chromatography (RP-HPLC, waters, e2695 system; 2489 UV/Vis detector)**.** If the process slowed down, extra portion of H_2O_2 (3.0 equiv.) was added until the completion of release. Similarly, other solutions of ibuprofen (40 μmmol/L), **11** (10 μmmol/L), and **12** (40 μmmol/L) were prepared in purified water and acetonitrile (50%:50%, V/V). All of the tests were detected on ODS column (250×4.6 mm, 5 μm) at different time points with an eluent of acetonitrile/water (10:90-100:0, 16 min; 100:0, 20 min; 50:50, V/V) (0.05 % trifluoroacetic acid in water). The volume of sample injection was 10 μL and the flow rate was 1 mL/min with column oven of 35 ^oC. All solutions prefiltered with 0.45 μm filter were detected using UV detector under 254 nm.

4.7. In vitro H_2O_2-eliminating capability

Various concentrations of trolox (1,5,10, 20, 30 μM), **22** (1,5,10, 20, 30 μM), ibuprofen (1,5,10, 20, 30 μM) and **11** (1,5,10, 20, 30 μM) were incubated in 4 mL PBS (7.4) containing 200 μM H_2O_2 at 37 ^oC for 24 h. The remaining H_2O_2 in various reaction solutions were detected via QuantiChrom Peroxide Assay Kit (DIOX-250, BioAssay Systems) while the scavenged H_2O_2 was calculated by graph pad prism 8.0. The relationship between consuming H_2O_2 and concentrations of various compounds were graphed via origin pro 2016.

4.8. Blood-brain barrier (BBB) permeation assays and cellular uptake

As for the blood-brain barrier permeation assays, b.End.3 cells at a density of 2×10^5 cells/cm^2 were seeded into the upper chamber of transwell while SH-SY5Y cells (1×10^5 cells/cm^2) were seeded into the lower chamber of transwell. All of the cells were cultured in monolayer. Trans-Endothelial electrical resistance (TEER) values of cells in upper chamber were monitored with voltammeter (Millipore) and

used for BBB assays until the TEER values reached more than 180 Ω•cm^2. Thereafter, **22** and **25** (10 μM) were added to the upper chamber, respectively and incubated for 2 h at 37 ^{o}C. The concentration of **22** in the lower culture medium was analyzed with HPLC. After another 6 h co-incubation, SH-SY5Y cells were collected, lysed with RIPA lysis buffer and cytoplasm was collected for HPLC detection. The concentration of **22** in SH-SY5Y cells calculated with Graph Pad Prism 8.0 and showed as one of three independent experiment. TEER= $(R_t-R_b)*A$, R_t and R_b represent the total resistance and background resistance, respectively, and A is the transwell area (0.33 cm^2). As for **25**, the cells in lower chamber were washed twice with cold PBS and gathered for images with laser confocal microscope.

As for uptake of **25**, SH-SY5Y or BV-2 cells were seeded onto six-well plates (1×10^5 cells/mL) and allowed to adhere at 37 ^{o}C for overnight. After 80 % confluence, the cells were treated with compound **25** (10 μM) for 12 h at 37 ^{o}C. Subsequently, the cells were washed twice with PBS, recorded and analyzed with laser scanning confocal microscope. (Ex. 405 nm, Em. 488 nm).

4.9. Immunofluorescence assays of ZO-1

BEnd.3 (5×10^5 cells/mL) cells were seeded into glass bottom cell culture dishes till the formation of monomer cells. Then the cells were treated with DMSO or **22** for 45 min. After that, the cells were washed with cold PBS, fixed in paraformaldehyde (4%) and permeabilized with 0.5% Triton X-100 in PBS. Then, the cells were labeled with primary antibodies (ab216880, abcam) followed with Alexa-Fluoro488-labeled goat anti-rabbit secondary antibody. The nuclei were stained with DAPI, while images were recorded and analyzed via laser confocal microscope. The results were shown as one of three independent experiments.

4.10. LPS-induced ROS accumulation assays

BV-2 cells were seeded onto six-well plates (1×10^5 cells/mL) and allowed to adhere overnight. After 80 % confluence, the cells were pretreated with compound **22** (10 μM), ibuprofen+**11** (10 μM + 10 μM) for 6 h followed with another 18 h co-treatment with LPS (3 μg/mL). Similarly, untreated cells (DMSO) and LPS (3 μg/mL)-treated cells were used as controls. BV-2 cells pretreated with LPS (3 μg/mL)

for 6 h followed with another 18 h co-incubation with **22** (10 μM) was also used as control. After 24 h co-treatment at 37 ^{o}C, the cells were trypsinized, collected for DCFH-DA staining at dark for 20 min and imaged via laser confocal microscope with the excitation wavelength and emission wavelength of 488 nm and 530 nm. Results were displayed as one of three independent experiments.

4.11. AChE inhibition study

The AChE inhibition was investigated with colorimetric method according to the research previously reported by Ellman et al [32,34]. The details of materials were as follows: AChE (EC3.1.1.7, Type VI−S, Electric Eel); (5,5'-Dithiobis-(2-nitrobenzoic acid)) DTNB (pH=8.0 Gluco Biotechnology Co., Ltd, Nanjing); acetylthiocholine chloride (ATC, Sigma Aldrich); tacrine (Sigma Aldrich). Tacrine and target compounds were dissolved in DMSO and diluted to 10^{-9}-10^{-5} M with 0.1 M NaH_2PO_4/Na_2HPO_4 buffer (pH 7.4). As for the measurement of AChE assay of target compounds under H_2O_2. Compounds **19**-**22** was dissolved in DMSO and diluted with PBS buffer to 40 mM followed with the addition of H_2O_2 (6.0 equiv.) and co-incubated for 10 h at 37 ^{o}C in dark. The release solution was diluted with PBS buffer to a final concentration range and used for the following assays.

For measurement, the AChE was diluted to 2.0 units/mL in 2 mL aliquots. After 5 min co-incubation of contained PBS (1 mL), AChE (10 μL), test compound solution (10 μL) and DTNB (0.01 M, 30 μL) at 25 ^{o}C, the reaction was started with acetylthiocholine chloride (0.01 M, 30 μL) and incubated for 1 min at 37 ^{o}C. The absorbance of various solution was recorded with enzyme-labeled instrument at 410 nm for three independent experiments. Similarly, pure water was tested as control. The IC_{50} values were calculated with Graph Pad Prism 6.0.

4.12. Molecular docking studies

The moleular docking were performed with Sybyl-X 2.0 (Sybyl-X 2.0 was available from state key laboratory for the chemistry and molecular engineering of medicinal resources of guangxi normal university). The structures used in this stdudies were constructed with chem 3D pro 14.0 followed by ennergy minimized with tripos force field, using optimization gradient of 0.001 kcal/mol·Å and a

maximum optimal step size of 1000. The crystal structure of torpedo californica AChE (PDB ID: 2CKM) was obtained from the RCSB protein data bank and modified with Sybyl-X 2.0. For preparing receptor protein, the water molecules were removed and the missing hydrogen atoms were added. The docking results were obtained in Sybyl-X 2.0 Surflex-Dock model. Besides, the docking parameters were kept as default values.

4.13. The detection of inflammatory factors in BV-2 cells by real-time quantitative PCR (qRT-PCR)

The effects of **22** on expression of inflammatory factors induced by H_2O_2 were detected by real-time quantitative PCR (qRT-PCR). BV-2 cells were seeded onto six-well plates (1×10^5 cells/mL) and allowed to adhere at 37 ^oC for overnight. When cells were 80% confluence, the cells were pre-treated with or without **22** (5 μM, 10 μM) for 6 h and treated with H_2O_2 (100 μM) for another 24 h at the same condition. The total RNA isolated with TRIzol reagent (Invitrogen Co., Carlsbad, CA), purified with chloroform and isopropanol and quantified with the NanoDrop 2000c spectrophotometer (ThermoFisher Scientific, Madrid, Spain) at 260/280 wavelength. After reverse transcription cDNA by a High Capacity RNA-to-cDNA kit (TOYOBO, Japan), real-time quantitative PCR was performed with 10 μL of final reaction volume including SYBR green I master mix. The method of amplification was carried out according to the previous report [47] and the results were analyzed with ΔΔCt method [48]. The primer sequences were used as follows: IL-1β R-AGC TCT CCA CCT CAA TGG AC; TNF-α R-CTG TAG CCC ACG TCG TAG; GAPDH R-CAC TGA GGA CCA GGT TGT CT

4.14. Apoptosis detection

The neuroprotective effects of compound 96 were studied using apoptosis assay. SH-SY5Y cells were seeded onto six-well plates (1×10^5 cells/mL) and allowed to adhere at 37 ^oC for overnight. The cells were pretreated with control (DMSO), compound 96 (5 μM and 10 μM) for 6 h at 37 ^oC. Then the cells were treated H_2O_2 (100 μM) and incubated for another 24 h at the same condition. Then both the

adherent and floating cells were collected, centrifuged (2000 rpm for 5 min) and washed twice with cold PBS. Lastly, the cells were resuspended with 500 μL binding buffer, stained with Annexin V-FITC (5 μL) and propidium iodide (5 μL) for 15 min at room temperature and analyzed with flow cytometry (Cell Quest; BD Biosciences).

4.15. Hepatotoxicity Studies

In order to investigate whether our target copunds obtained decreased hepatotoxicity in coparison to tacrine. ROS accumulation assays induced by **22** or tacrine were measured. Briefly, Hep G2 were seeded onto six-well plates (1×10^5 cells/mL) and allowed to adhere at 37 ^oC for overnight. Subsequently, the cells were treated with control (DMSO), compound **22** (25 μM and 50 μM) and tacrine (50 μM) at 37 ^oC for another 24 h. Thereafter, the cells were washed twice with cold PBS, stained with ROS tracker followed by washing with PBS. The accumulation of ROS was recorded and analyzed with laser confocal microscope (Ex. 490 nm/Em. 535 nm).

4.16. Cell morphology assay

The cell morphology assay was detected with cytotoxicity assay kit (KGAF001, KeyGEN BioTECH). SH-SY5Y cells were seeded onto six-well plates (1×10^5 cells/mL) and allowed to adhere at 37 ^oC for overnight. Then the cells were treated with control (DMSO), compound **22** (5 μM and 10 μM) for 6 h at 37 ^oC. Subsequently, the cells were treated with H_2O_2 (100 μM) and incubated for another 24 h at the same condition. Lastly, the cells were stained with calcein AM/PI probe prepared according to the illustration of the manufacture for 30 min in dark at room temperature. The cells were washed twice with cold PBS and analyzed with laser confocal microscope.

4.17. Western blotting assay

In order to investigate the expression of related protein in the mitochondrial apoptosis pathway, the western blotting study was performed. SH-SY5Y cells were seeded into six-well plates at a density of 1×10^5 cells/mL and allowed to adhere at 37 ^oC for overnight. Thereafter, the cells were pre-incubated with different conditions, including **22** (5 μM and 10 μM), control (DMSO) for 6 h. Then the cells were exposed to H_2O_2 (100 μM) (one group of control was not treated) and incubated for another 24

h at the same condition. The cells were harvested and lysed with RIPA lysis buffer (KGP703/KGP703-100, KeyGEN BioTECH) at 4 °C for 30 min. Lysates were centrifuged at 15000 rpm for 15 min at 4 °C and collected the supernatants. Protein concentration was quantified by BCA protein assay kit (KGPBCA, KeyGEN BioTECH). Equal protein samples were loaded on 10−12% SDS-PAGE, electrophoretically transferred onto polyvinylidenedifluoride (PVDF) Hybond-P membranes and blocked with 5% nonfat milk. The membranes were subsequently incubated with primary antibodies (anti-Bcl-2, anti-Bax, anti-caspase-3 and anti-β-actin) with the dilutions. Lastly, the membranes were incubated with appropriate secondary antibody and visualized with enhanced chemiluminescence kit (Thermo Fischer Scientifics Ltd.). The expression of each protein were recorded and analyzed with Image software normalizing with β-actin.

4.18. Morris water maze (MWM) assay

Male SD rats were purchased from Shanghai Slac Laboratory Animal Co., Ltd. (China), housed in the facility at the Laboratory Animal Center, Academy of Simcere according to the guidelines approved for laboratory animals. All surgical interventions and postoperative animal care procedures were approved by the Experimental Animal Ethics Committee of Southeast University (Nanjing, China).

$A\beta_{25-35}$ (Sigma) was stored in saline and incubated at 37 °C in dark for 7 days to obtain the aggregated form and thereafter was diluted to final concentration of 5 μg/μL. The model of AD in rats was established according to previous reports [4]. After one-week habituation period (25 ± 1 °C, 55% of humidity, natural light/dark conditions), total 15 rats were slowly injected aggregated $A\beta_{25-35}$ (2 μL, 5 μg/μL) in the hippocampus under anesthesia of chloral hydrate (7%, intraperitoneal injection) at the following coordinates: right hippocampus (−3.8 mm AP, −2.5 mm ML, and −3.2 mm DV, according to the Rat Brain Paxinos Atlas). The injection lasted for 2 min (1 μL/min) and the needle was slowly withdrawn after 8 min remaining of complete infusion. These rats were allowed for another week recovery. Thereafter, they were randomly divided into three groups (n=5) and treated daily intraperitoneal injection of tacrine (1.0 μmol/100g b.wt.,0.2 mg/100g, qd), **22** (1.0 μmol/100g b.wt.,0.9 mg/100g,

qd), using equal amount of normal saline for control group. 28 days later, morris water maze task was carried out to investigate the therapeutic effects of our target **22**, using in a circular tank (diameter, 125 cm; height, 30 cm) equipped with a platform of 9 cm in diameter and 2 cm below the opacified water surface in the middle of a northeast quadrant. Before starting the MWM assays, the rats were received memory training for four trials per day and a 30 min interval to find the hidden platform in the following 5 days. In the single test, each rat of three different groups was placed in one of the quadrant and faced the wall. Moreover, the position of each rat varied in the consecutive 5 days. If the rat succeeded to find the hidden platform, the animal was allowed to stay on the platform for 10 s. If not, the animal was guided to find the platform and allowed it to stay on the platform for 10 s. The escape latency and trajectories were record and analyzed with computerized video-tracking system.

After the last memory training, the hidden platform was removed. In order to investigate the therapeutic effect on memory retention of the rats in different groups. Each rat was allowed to swim freely in 90 s in the tank (for only one trial) and the starting location was from the southwest. The swimming path of rats looked for the platform (target platform) and the number of times it crossed the platform where use to be were record and analyzed with computerized digitalizing video-tracking system.

NOTES

The authors declare that they have no conflicts of interest.

ACKNOWLEDGEMENTS

The authors are grateful to Jiangsu Province Hi-tech Key Laboratory for Biomedical Research for financial aids to this research. We appreicate Jiangsu KeyGen Biotech Company for in vivo tests. We also want to thank to Prof. Hengshan Wang (Guangxi Normal University) for a license to use their software (Sybyl-X 2.0). Dr. Fang is thankful to the support of the State Key Laboratory for Chemistry and Molecular Engineering of Medicinal Resources (Guangxi Normal University)

(CMEMR2017-B05), and “Qing-Lan” project in Colleges and Universities of Jiangsu Province.

APPENDIX A. Supporting Information

Supporting Information supplemental figures were available via the internet.

The preparation of tacrine derivatives **8**-**11**; General synthetic procedures for the target compound **25**; In vitro H_2O_2-scavenging capacity and the release of ibuprofen and tacrine derivative **11**; Envisaged mechanism of **22** degraded in D_2O triggered by H_2O_2; Oxidation mechanism of **22** triggered by H_2O_2; Transendothelial cell electrical resistance (TEER) assays; Blood-brain barrier (BBB) permeation assays; **22** reduced intracellular accumulation ROS induced by LPS; ^{1}H-NMR, ^{13}C- NMR and HR-MS spectra of the target compounds; Purity measurements by HPLC.

ABBREVIATIONS USED

AD, Alzheimer’s disease; Aβ, amyloid-β; MTDLs, multi-target-directed ligands; AChE, acetylcholinesterase; BBB, blood-brain-barrier; NMDAR, N-methyl-D-aspartate receptor; DA, dopamine; O_2, oxygen; ROS, reactive oxygen species; $O^{2\bullet-}$, superoxide anion radical; H_2O_2, hydrogen peroxide; CDI, N,N'-carbonyldiimidazole; DMF, N,N-dimethylformamide; NSAIDs, nonsteroidal anti-inflammatory drugs; MTT, thiazolyl blue tetrazolium bromide; SH-SY5Y, human neuroblastoma cells; RP-HPLC, reverse phase high performance liquid chromatography; TEER, transendothelial electrical resistance; TJ, tight junction; CAS, catalytic active site; PAS, peripheral active site; LPS, lipopolysaccharide; MWM, morris water maze.

REFERENCES

[1] R.S. Wilson, E. Segawa, P.A. Boyle, S.E. Anagnos, L.P. Hizel, D.A. Bennett, The natural history of cognitive decline in Alzheimer’s disease, Psychol Aging 27 (2012) 1008–1017.

[2] W.W. Barker, C.A. Luis, A. Kashuba, M. Luis, D.G. Harwood, D. Loewenstein, C. Waters, P. Jimison, E. Shepherd, S. Sevush, N. Graff-Radford, D. Newland, M. Todd, B. Miller, M. Gold, K. Heilman, L. Doty, I. Goodman, B. Robinson, G. Pearl, D.

Dickson, R. Duara, Relative frequencies of Alzheimer's disease, lewy body, vascular and frontotemporal dementia, and hippocampal sclerosis in the State of Florida Brain Bank, Alzheimer Dis. Assoc. Disord. 16 (2002) 203–212.

[3] https://www.alz.co.uk/research/world-report-2018, The state of the art of dementia research: new frontiers.

[4] Alzheimer's association international conference 2019, Alzheimers Dement. 15 (2019) 321−387.

[5] H. Zheng, M. Fridkin, M. Youdim, New approaches to treating Alzheimer's disease, Perspect. Med. Chem. 7 (2015) 1−8.

[6] C. Ríos, J. Marco-Contelles, Tacrines for Alzheimer's disease therapy. III. the pyrido tacrines, Eur. J. Med. Chem. 166 (2019) 381−389.

[7] V. Echeverria, A. Yarkov, G. Aliev, Positive modulators of the α7 nicotinic receptor against neuroinflammation and cognitive impairment in Alzheimer's disease, Prog. Neurobiol. 144 (2016)142−157.

[8] A. Sierra, S. Beccari, I. Diaz-Aparicio, J.M. Encinas, S. Comeau, M.E. Tremblay, Surveillance, phagocytosis, and inflammation: how never-resting microglia influence adult hippocampal neurogenesis, Neural Plast. 2014 (2014) 142-157.

[9] Z. Wang, J. Hu, X. Yang, X. Feng, X. Li, L. Huang, A.S.C. Chan, Design, synthesis, and evaluation of orally bioavailable quinoline−indole derivatives as innovative multitarget-directed ligands: promotion of cell proliferation in the adult murine hippocampus for the treatment of alzheimer's disease, J. Med. Chem. 61 (2018) 1871−1894.

[10] I. Sola, E. Aso, D. Frattini, I. López-Gonzalez, A. Espargaro, R. Sabaté, O. Di Pietro, F.J. Luque, M.V. Clos, I. Ferrer, D. Munoz-Torrero, Novel levetiracetam derivatives that are effective against the Alzheimer-like phenotype in mice: synthesis, in vitro, ex vivo, and in vivo efficacy studies, J. Med. Chem. 58 (2015) 6018−6032.

[11] H. Lee, S. Fan, F. Huang, H. Chao, K. Hsu, T.E. Lin, T. Yeh, M. Lai, Y. Li, H. Huang, C. Yang, J. Liou, 5‐aroylindoles act as selective histone deacetylase 6 inhibitors ameliorating Alzheimer's disease phenotypes, J. Med. Chem. 61 (2018) 7087−7102.

[12] R. Farina, L. Pisani, M. Catto, O. Nicolotti, D. Gadaleta, N. Denora, R. Soto-Otero, E. Mendez-Alvarez, C.S. Passos, G. Muncipinto, C.D. Altomare, A. Nurisso, P.A. Carrupt, A. Carotti, Structure-based design and optimization of multitarget-directed 2H-chromen-2-one derivatives as potent inhibitors of monoamine oxidase B and cholinesterases, J. Med. Chem. 58 (2015) 5561−5578.

[13] E. Viayna, I. Sola, M. Bartolini, A. De Simone, C. Tapia-Rojas, F.G. Serrano, R. Sabate, J. Juarez-Jimenez, B.; Perez, F.J. Luque, V. Andrisano, M.V. Clos, N.C. Inestrosa, D. Munoz-Torrero, Synthesis and multitarget biological profiling of a novel family of rhein derivatives as disease-modifying anti-Alzheimer agents, J. Med. Chem. 57 (2014) 2549−2567.

[14] M. Awasthi, S. Singh, V.P. Pandey, U.N. Dwivedi, Alzheimer's disease: An overview of amyloid beta dependent pathogenesis and its therapeutic implications along with in silico approaches emphasizing the role of natural products, J. Neurol. Sci. 361 (2016) 256−271.

[15] P. Chen, W. Tsai, Y. Ueng, T. Tzeng, H. Chen, P. Zhu, C. Huang, Y. Shiao, W. Li, Neuroprotective and antineuroinflammatory effects of hydroxyl-functionalized stilbenes and 2‑arylbenzo[b]furans, J. Med. Chem. 60 (2017) 4062−4073.

[16] A.F. McKoy, J. Chen, T. Schupbach, M.H. Hecht, A novel inhibitor of amyloid β (Aβ) peptide aggregation: from high throughput screening to efficacy in an animal model of Alzheimer disease, J. Biol. Chem. 287 (2012) 38992−39000.

[17] A.L. Lublin, C.D. Link, Alzheimer's disease drug discovery: In vivo screening using caenorhabditis elegans as a model for β-amyloid peptide-induced toxicity. Drug Discovery Today: Technol, 10 (2013) e115−e119.

[18] M. Rosini, E. Simoni, A. Milelli, A. Minarini, C. Melchiorre, Oxidative stress in Alzheimer's disease: are we connecting the dots? J. Med. Chem. 57 (2014) 2821−2831.

[19] R. von Bernhardi, J. Eugenin, Alzheimer's disease: redox dysregulation as a common denominator for diverse pathogenic mechanisms, Antioxid. Redox Sign. 16 (2012) 974−1031.

[20] E. Nam, J.S. Derrick, S. Lee, J. Kang, J. Han, S.J.C. Lee, S.W. Chung, M.H. Lim,

Regulatory activities of dopamine and its derivatives toward metal-free and metal-induced Amyloid‐β aggregation, oxidative stress, and inflammation in Alzheimer's disease, ACS Chem. Neurosci. 9 (2018) 2655−2666.

[21] J. Segura-Aguilar, I. Paris, P. Muñoz, E. Ferrari, L. Zecca, F.A. Zucca, Protective and toxic roles of dopamine in Parkinson's disease, J. Neurochem. 129 (2014) 898−915.

[22] W. Linert, E. Herlinger, R.F. Jameson, E. Kienzl, K. Jellinger, M.B. Youdim, Dopamine, 6-hydroxydopamine, iron, and dioxygen−their mutual interactions and possible implication in the development of Parkinson's disease, Biochim. Biophys. Acta. 1316 (1996) 160−168.

[23] J.I. Rossato, L.R.M. Bevilaqua, I. Izquierdo, J.H. Medina, M. Cammarota, Dopamine controls persistence of long-term memory storage, *Science* 325 (2009) 1017−1020.

[24] S.D. Mhatre, C.A. Tsai, A.J. Rubin, M.L. James, K.I. Andreasson, Microglial malfunction: the third rail in the development of alzheimer's disease, Trends Neurosci. 38 (2015) 621−636.

[25] N.S. Woodling, K.I. Andreasson, Untangling the web: toxic and protective effects of neuroinflammation and PGE2 signaling in Alzheimer's disease, ACS Chem. Neurosci. 7 (2016) 454−463.

[26] M.W. Salter, B. Stevens, Microglia emerge as central players in brain disease, Nat. Med. 23 (2017) 1018-1027.

[27] (a) A.R. Lippert, G.C. Van de Bittner, C.J. Chang, Boronate oxidation as a bioorthogonal reaction approach for studying the chemistry of hydrogen peroxide in living systems, Acc. Chem. Res. 44 (2011) 793−804. (b) C. de Gracia Lux, S. Joshi-Barr, T. Nguyen, E. Mahmoud, E. Schopf, N. Fomina, A. Almutairi, Biocompatible polymeric nanoparticles degrade and release cargo in response to biologically relevant levels of hydrogen peroxide, J. Am. Chem. Soc. 134 (2012) 15758−15764.

[28] A. Pettignano, S. Grijalvo, M. Haring, R. Eritja, N. Tanchoux, F. Quignard, D.D.

Diáz, Boronic acid-modified alginate enables direct formation of injectable, self-healing and multistimuliresponsive hydrogels, Chem. Commun. 53 (2017) 3350−3353.

[29] B. Yang, Y. Chen, J. Shi, Reactive oxygen species (ROS)-based nanomedicine, Chem. Rev. 119 (2019) 4881−4985.

[30] M.L. Viger, G. Collet, J. Lux, V.A. Nguyen Huu, M. Guma, A. Foucault-Collet, J. Olejniczak, S. Joshi-Barr, G.S. Firestein, A. Almutairi, Distinct on/off fluorescence signals from dualresponsive activatable nanoprobes allows detection of inflammation with improved contrast, Biomaterials 133 (2017) 119−131.

[31] L. Fang, D. Appenroth, M. Decker, M. Kiehntopf, A. Lupp, S. Peng, C. Fleck, Y. Zhang, J. Lehmann, NO-donating tacrine hybrid compounds improve scopolamine-induced cognition impairment and show less hepatotoxicity, J. Med. Chem. 51 (2008) 7666–7669.

[32] (a) L. Fang, B. Kraus, J. Lehmann, J. Heilmann, Y. Zhang, M. Decker, Design and synthesis of tacrine–ferulic acid hybrids as multi-potent anti-Alzheimer drug candidates, Bioorg. Med. Chem. Lett. 18 (2008) 2905–2909. (b) M.L. Bolognesi, A. Cavalli, L. Valgimigli, M. Bartolini, M. Rosini, V. Andrisano, M. Recanatini, C. Melchiorre, Multi-target-directed drug design strategy: from a dual binding site acetylcholinesterase inhibitor to a trifunctional compound against Alzheimer's disease, J. Med. Chem. 50 (2007) 6446-6449. (c) M. Przybyłowska, S. Kowalski, K. Dzierzbicka, I. Inkielewicz-Stepniak, Therapeutic potential of multifunctional tacrine analogues, Curr. Neuropharmacol. 17 (2019) 472-490.

[33] (a) L.A. Kotilinek, M.A. Westerman, Q. Wang, K. Panizzon, G. P. Lim, A. Simonyi, S. Lesne, A. Falinska, L.H. Younkin, S.G. Younkin, M. Rowan, J. Cleary, R.A. Wallis, G.Y. Sun, G. Cole, S. Frautschy, R. Anwyl, K. H. Ashe, Cyclooxygenase-2 inhibition improves amyloid-beta-mediated suppression of memory and synaptic plasticity, Brain 131 (2008) 651−664. (b) G.P. Lim, F. Yang, T. Chu, P. Chen, W. Beech, B. Teter, T. Tran, O. Ubeda, K.H. Ashe, S.A. Frautschy, G.M. Cole, Ibuprofen suppresses plaque pathology and inflammation in a mouse model for Alzheimer's disease, J. Neurosci. 20 (2000) 5709-5714.

[34] (a) S. Weggen, J.L. Eriksen, P. Das, S.A. Sagi, R. Wang, C.U. Pietrzik, K.A. Findlay, T.E. Smith, M.P. Murphy, T. Bulter, D.E. Kang, N. Marquez-Sterling, T.E. Golde, E.H. Koo, A subset of NSAIDs lower amyloidogenic Abeta42 independently of cyclooxygenase activity, Nature 414 (2001) 212−216 (b) D. Patela, A. Roya, M. Kundua, M.Janaa, C.H. Luanc, F.J. Gonzalezd, K. Pahan, Aspirin binds to PPARα to stimulate hippocampal plasticity and protect memory, Proc. Natl. Acad. Sci. USA 2018: 201802021 (c) G. Lim, F. Yang, T. Chua, E. Gahtanb,O. Ubedaa, W. Beecha, J.B. Overmierb, K. Hsiao-Ashec, S.A. Frautschya, G.M. Colea, Ibuprofen effects on Alzheimer pathology and open field activity in APPsw transgenic mice. Neurobiol. Aging 22 (2001) 983-991. (d) B.L. Wilkinson, P.E. Cramer, N.H. Varvel, E. Reed-Geaghan, Q. Jiang, A. Szabo, K. Herrup, B.T. Lamb, G.E. Landreth, Ibuprofen attenuates oxidative damage through NOX2 inhibition in Alzheimer's disease, Neurobiol. Aging 33 (2012) 197.e121-197.e132.

[35] (a) Z. Wang, Y. Wang, B. Wang, W. Li, L. Huang, X. Li, Design, synthesis, and evaluation of orally available clioquinol-moracin M hybrids as multitarget-directed ligands for cognitive improvement in a rat model of neurodegeneration in alzheimer's disease, J. Med. Chem. 58 (2015) 8616−8637. (b) D. Wu, M. Qin, D. Xu, L. Wang, C.Liu, J. Ren, G. Zhou, C. Chen, F. Yang, Y. Li, Y. Zhao, R. Huang, S. Pourtaheri, C. Kang, M. Kamata, I.S.Y. Chen, Z. He, J. Wen, W. Chen, Y. Lu, A bioinspired platform for effective delivery of protein therapeutics to the central nervous system, Adv. Mater. 31(2019) 1807557.

[36] (a) M. von Wedel-Parlow, S. Schrot, J. Lemmen, L. Treeratanapiboon, J. Wegener, H.J. Galla, Neutrophils cross the BBB primarily on transcellular pathways: an in vitro study, Brain Res. 1367 (2011) 62–76. (b) H. Singh, S.J. Kim, D.H. Kang, H.R. Kim, A. Sharma, W.Y. Kim, C. Kang, J.S. Kim, Glycyrrhetinic acid as a hepatocyte targeting unit for an anticancer drug delivery system with enhanced cell type selectivity, Chem. Commun. 54 (2018) 12353−12356.

[37] I.S. Marks, S.S. Gardeen, S.J. Kurdziel, S.T. Nicolaou, J.E. Woods, S.A. Kularatne, P.S. Low, Development of a small molecule tubulysin B conjugate for treatment of carbonic anhydrase IX receptor expressing cancers, Mol. Pharmaceut. 15

(2018) 2289−2296.

[38] G.L. Ellman, K.D. Courtney,V.A. Jr. R.M. Featherstone, A new and rapid colorimetric determination of acetylcholinesterase activity, Biochem. Pharmacol. 7 (1961) 88−95.

[39] (a) J.W. Guo, P.P. Guan, W.Y. Ding, S.L. Wang, X.S. Huang, Z.Y. Wang, P. Wang, Erythrocyte membrane-encapsulated celecoxib improves the cognitive decline of Alzheimer's disease by concurrently inducing neurogenesis and reducing apoptosis in APP/PS1 transgenic mice, Biomaterials 145 (2017) 106−127. (b) Y.W. Tang, C.J. Shi, H.L. Yang, P. Cai, Q.H. Liu, X.L. Yang, L.Y. Kong, X.B. Wang, Synthesis and evaluation of isoprenylation-resveratrol dimer derivatives against Alzheimer's disease, Eur. J. Med. Chem. 163 (2019) 307-319. (c) S. Sil, T. Ghosh, R. Ghosh, P. Gupta, Nitric oxide synthase inhibitor, aminoguanidine reduces intracerebroventricular colchicine induced neurodegeneration, memory impairments and changes of systemic immune responses in rats, J. Neuroimmunol. 303 (2016) 51-61.

[40] W. Zhou, G. Zhong, S. Fu, H. Xie, T. Chi, L. Li, X. Rao, S. Zeng, D. Xu, H. Wang, G. Sheng, X. Ji, X. Liu, X. Ji, D. Wu, L. Zou, M. Tortorella, K. Zhang, W. Hu, Microglia-based phenotypic screening identifies a novel inhibitor of neuroinflammation effective in Alzheimer’s disease models, ACS Chem. Neurosci. 7 (2016)1499−1507

[41] T. Wyss-Coray, Inflammation in Alzheimer disease: driving force, bystander or beneficial response? Nat. Med. 12 (2006) 1005−1015.

[42] A. Romero, R. Cacabelos, M.J. Oset-Gasque, A. Samadi, J. Marco-Contelles, Novel tacrine-related drugs as potential candidates for the treatment of Alzheimer's disease, Bioorg. Med. Chem. Lett. 23 (2013) 1916−1922.

[43] R. Leon, A.G. García, J. Marco-Contelles, Recent advances in the multitarget-directed ligands approach for the treatment of Alzheimer's disease, Med. Res. Rev. 33 (2013) 139−189.

[44] Y. Chen, J. Sun, L. Fang, M. Liu, S. Peng, H. Liao, J. Lehmann, Y. Zhang, Tacrine−ferulic acid−nitric oxide (NO) donor trihybrids as potent, multifunctional acetyl- and butyrylcholinesterase inhibitors, J. Med. Chem. 55 (2012) 4309−4321.

[45] C.C. Hsu, J.C. Lien, C.W. Chang, C.H. Chang, S.C. Kuo, T.F. Huang, Yuwen02f1 suppresses LPS-induced endotoxemia and adjuvant-induced arthritis primarily through blockade of ROS formation, NFκB and MAPK activation, Biochem. Pharmacol. 85 (2013) 385–395.

[46] K.J. Wu, H.J. Zhong, G. Li, C. Liu, H.M.D. Wang, D.L. Ma, C.H. Leung, Structure-based identification of a NEDD8-activating enzyme inhibitor via drug repurposing, Eur. J. Med. Chem. 143 (2018) 1021−1027.

[47] X. Cheng, J. Gu, Y. Pang, J. Liu, T. Xu, X. Li, Y. Hua, K.A. Newell, X. Huang, Y. Yu, Y. Liu, Tacrine−hydrogen sulfide donor hybrid ameliorates cognitive impairment in the aluminum chloride mouse model of Alzheimer's disease, ACS Chem. Neurosci. 10 (2019) 3500 – 3509.

[48] J.d. Pino, J. Marco-Contelles, F. López-Muñoz, A. Romero, E. Ramos, Neuroinflammation signaling modulated by ASS234, a multitarget small molecule for alzheimer's disease therapy, ACS Chem. Neurosci. 9 (2018) 2880−2885.

Scheme 1. The preparation of target compounds.[1]

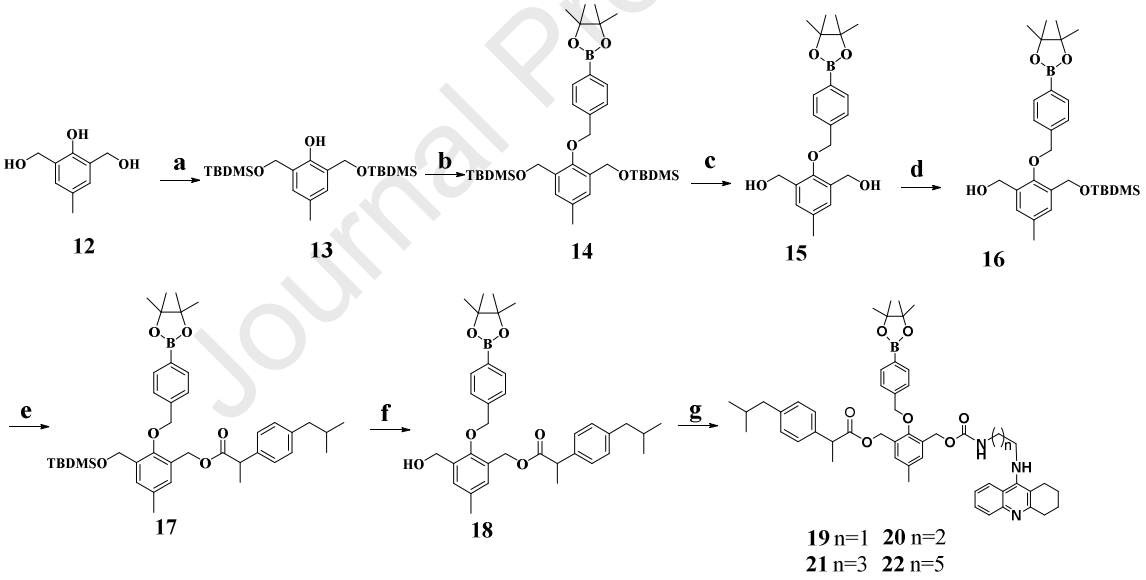

[1]**Reagents and conditions.** a) TBDMSCl, imidazole, DMF; b) 2-(4-(bromomethyl)benzyl)-4,4,5,5 -tetramethyl-1,3,2-dioxaborolane, K_2CO_3, DMF; c) PTSA, MeOH; d) TBDMSCl, imidazole, DMF; e) DCC, DMAP, Ibuprofen, DCM; f) PTSA, MeOH; g) CDI, DMF, **8** – **11.**

Figures:

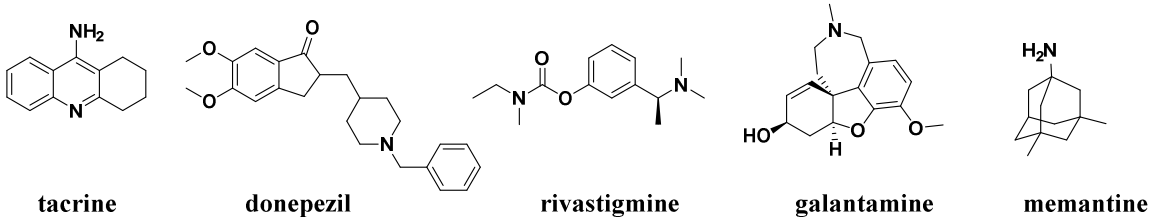

Figure 1. Drugs approved by FDA for AD treatment.

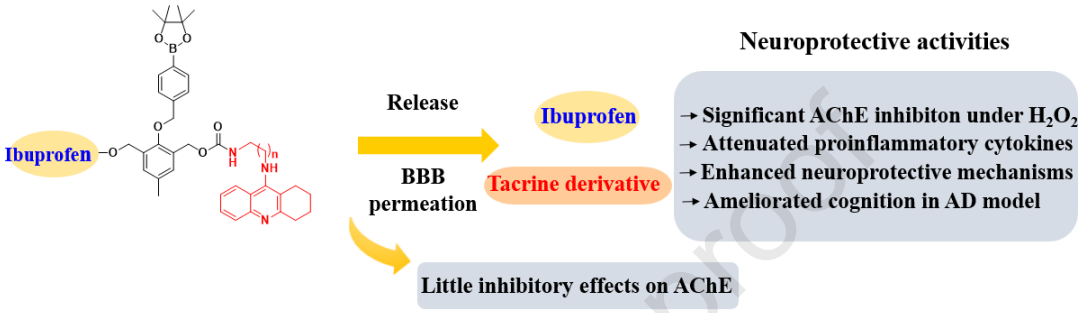

Figure 2. Design strategy of ROS-responsive prodrugs.

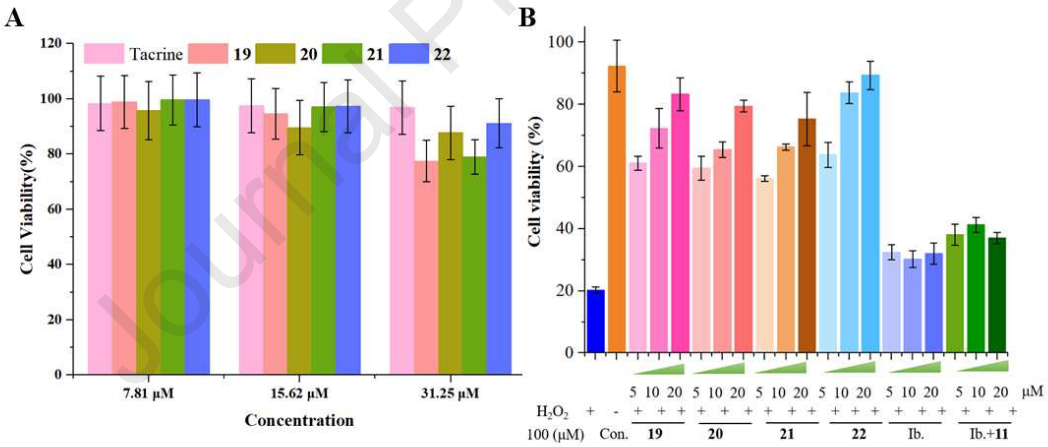

Figure 3. Cytotoxicity and neuroprotective effects against H_2O_2 assays. (A) SH-SY5Y cells were incubated with compounds **19-22** for 72 h at 37 ^{o}C. (B) SH-SY5Y cells were preincubated with compounds **19-22** for 6 h at 37 ^{o}C and subsequently treated with H_2O_2 (100 μM) for another 24 h. Ibuprofen and combined group (Ibuprofen+**11**) were used as controls. Results were shown as mean ± SD of three independent tests with MTT method.

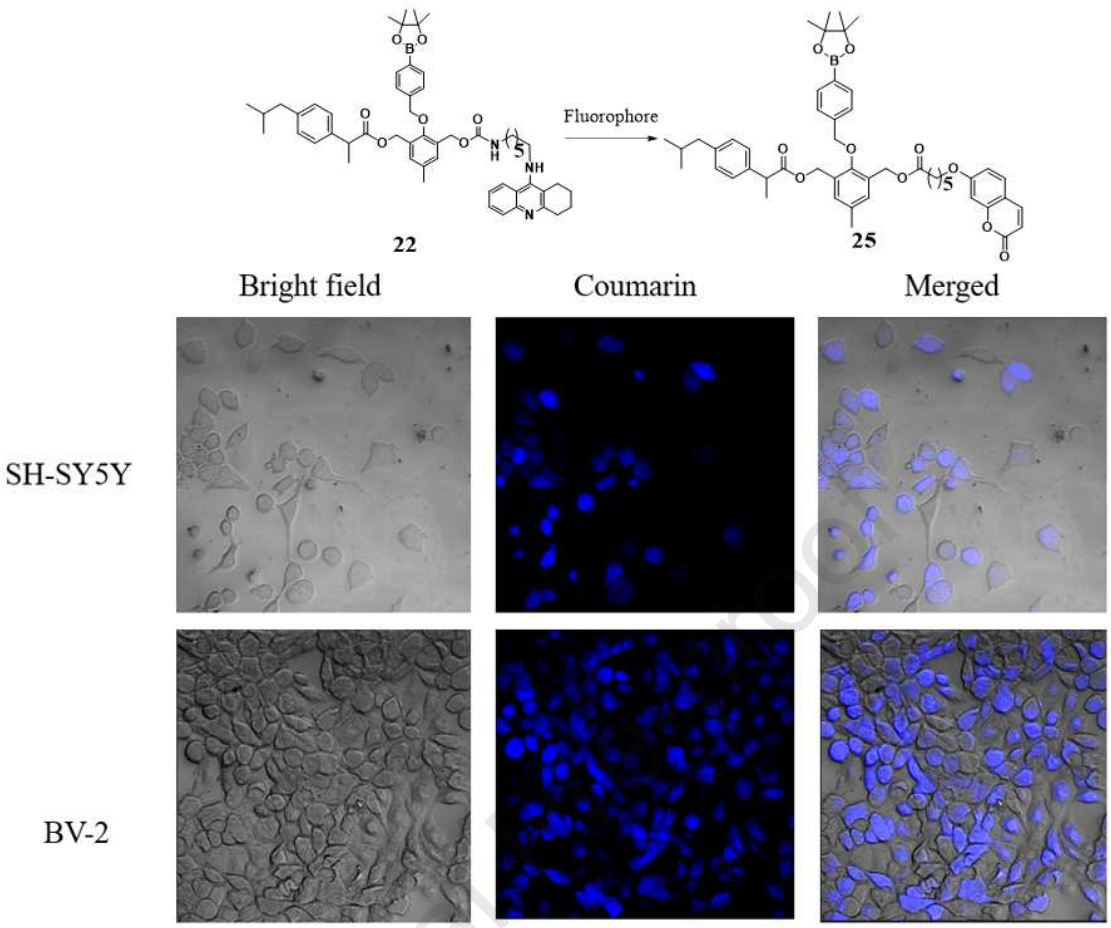

Figure 4. Cellular uptake of **25** in SH-SY5Y cells and BV-2 cells. After 12 h co-incubation with **25**, the images were obtained from laser confocal microscope. Cellular uptake of **25** in SH-SY5Y cells and in BV-2 cells. Results were shown as one of three independent experiments.

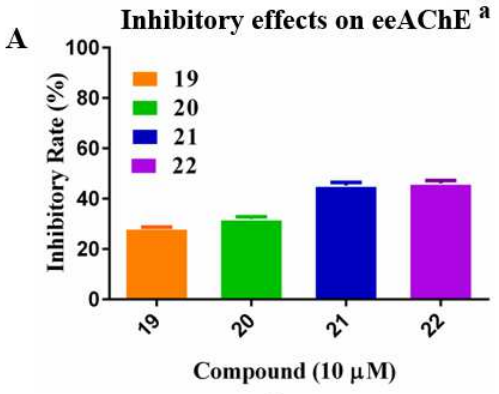

Inhibitory activities of eeAChE

Compd.	Inhibition Rate (%) [b]
19	28.25 ± 0.43
20	32.88 ± 0.95
21	45.99 ± 1.29
22	47.25 ± 1.18

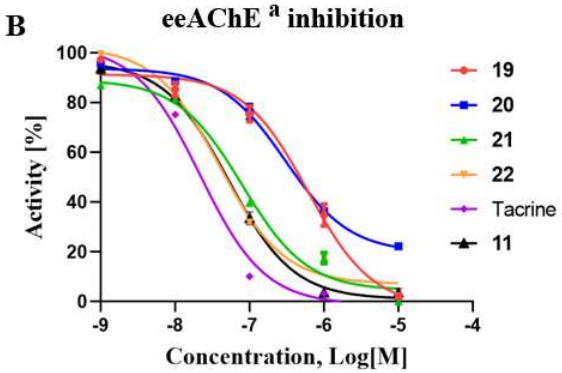

Inhibitory activities of eeAChE by 19-22 under H_2O_2

Compd.	IC_{50} (nM) [c]
19	608.1 ± 3.74
20	302.0 ± 1.55
21	80.02 ± 2.99
22	39.16 ± 3.00
Tacrine	21.63 ± 3.46
11	54.58 ± 1.37

Figure 5. The AChE inhibitory activity of the target compounds assayed by Ellman reaction at 37 ^{o}C. (A) [a] eeAChE from electric eel was used. Inhibitory effects on eeAChE of compounds **19**-**22** (10 μM) in the absence of H_2O_2, and [b] results were shown as mean ± SD of control group (DMSO). (B) Inhibitory activities of **19**-**22** on AChE in the presence of H_2O_2 (6 equiv.) after 10 h co-incubation. [a] eeAChE from electric eel was used. [c] Data were presented as mean ± SEM with three independent experiments.

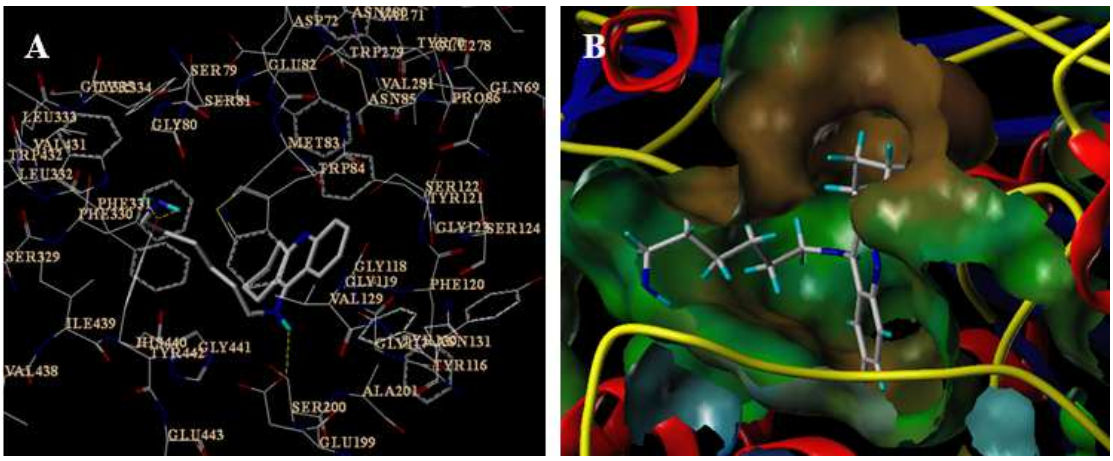

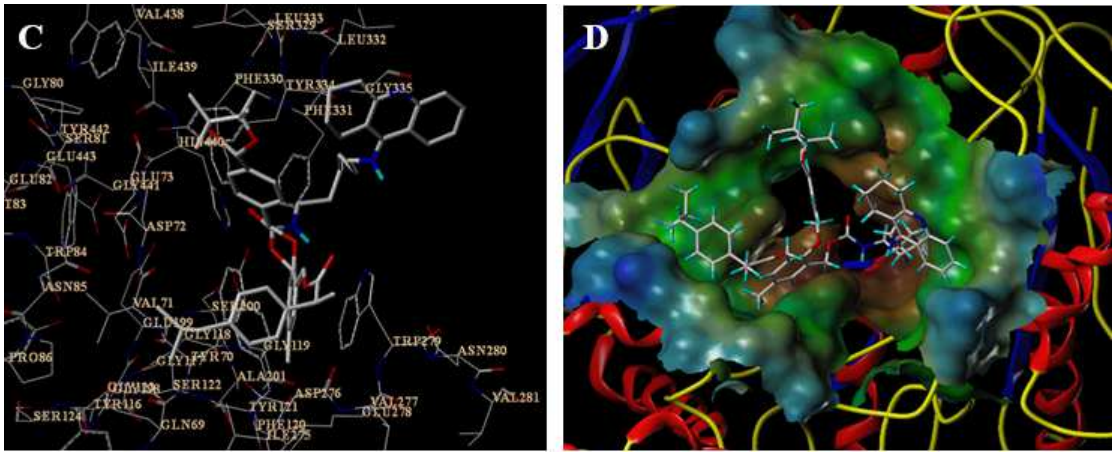

Figure 6. Representation of the binding model of **11** (A, B) and **22** (C, D) with torpedo californica AChE (2CKM), respectively. The binding pockets the binding sites are shown as stick model (A, C), while AChE was shown as secondary structure in ribbon model (B, D).

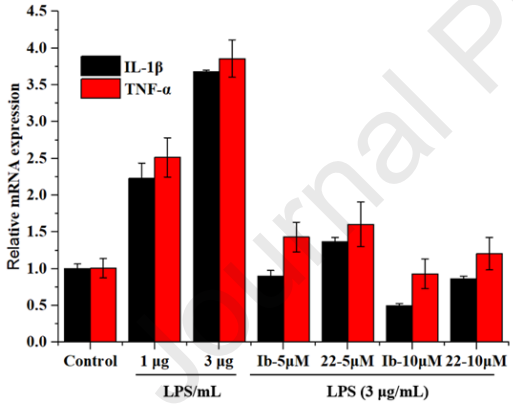

Relative mRNA expression[a]		
Compd.	IL-1β	TNF-α
Control	1.00 ± 0.064	1.00 ± 0.13
LPS(1μg/mL)	2.22 ± 0.21	2.51 ± 0.27
LPS(3μg/mL)	3.68 ± 0.020	3.86 ± 0.25
Ib-5μM[b]	0.90 ± 0.082	1.43 ± 0.20
22-5μM[b]	1.36 ± 0.065	1.60 ± 0.30
Ib-10μM[b]	0.49± 0.032	0.93 ± 0.20
22-10μM[b]	0.86 ± 0.035	1.20 ± 0.22

Figure 7. Compound **22** attenuated proinflammatory cytokines (TNF-α and IL-β). BV-2 cells were pretreated with **22** for 6 h followed with another 24 h co-incubation with LPS (3 μg/mL). [a] The results were expressed as mean ± SEM (n = 3) and normalized with control. [b] BV-2 cells were pre-treated with iburopfen (5 μM, 10 μM) or **22** (5 μM, 10 μM) for 6 h and then stimulated with LPS (3 μg/mL) for another 24 h at the same condition.

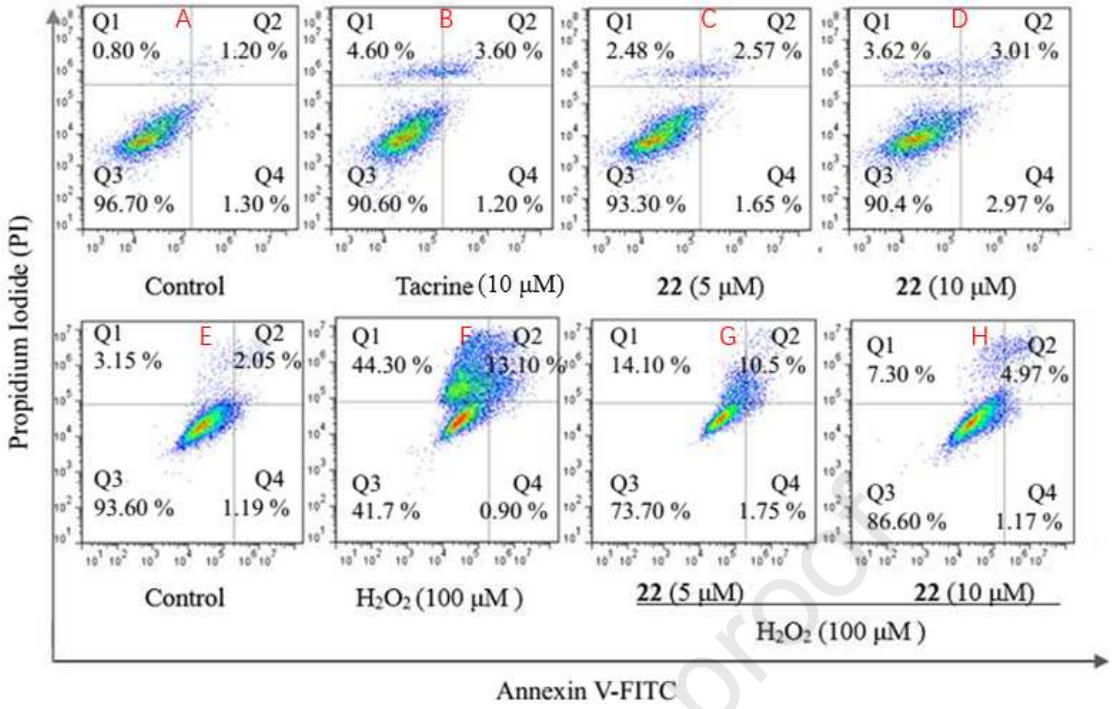

Figure 8. Cytoprotection effects of **22** against H_2O_2 in vitro. Apoptosis rates of SH-SY5Y cells after 24 h co-incubation with DMSO (A), tacrine (10 μM) (B), **22** (5 μM) (C), and **22** (10 μM) (D), respectively. SH-SY5Y cells were incubated with **22** (5 μM) (G) and **22** (10 μM) (H) for 6 h, then all of the cells were treated with DMSO (E), H_2O_2 (100 μM) (F-H) for another 24 h at 37 ^{o}C. The apoptotic rates of SH-SY5Y cells were obtained with flow cytometry. Results were presented as one of three independent experiments.

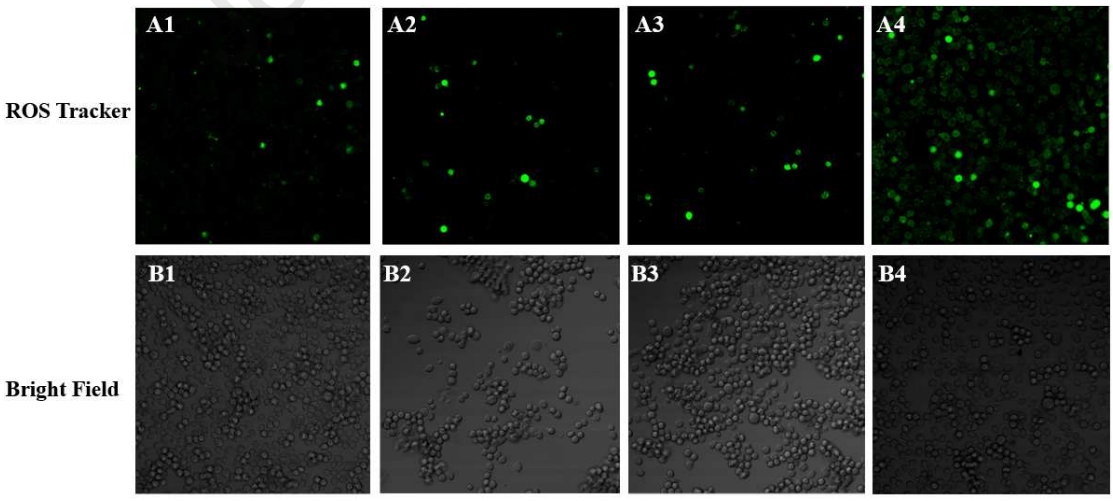

Figure 9. ROS accumulation assays in HepG2 induced by **22**, using tacrine as positive control. Hep G2 cells were treated differently as follows: DMSO (A1, B1), **22** (25 μM) (A2, B2), **22** (50 μM) (A3, B3), tacrine (50 μM) (A4, B4). After 24 h co-treatment, the cells were stained with

DCFH-DA, analyzed and recorded with laser confocal microscope (Ex. 490 nm, Em. 535 nm).

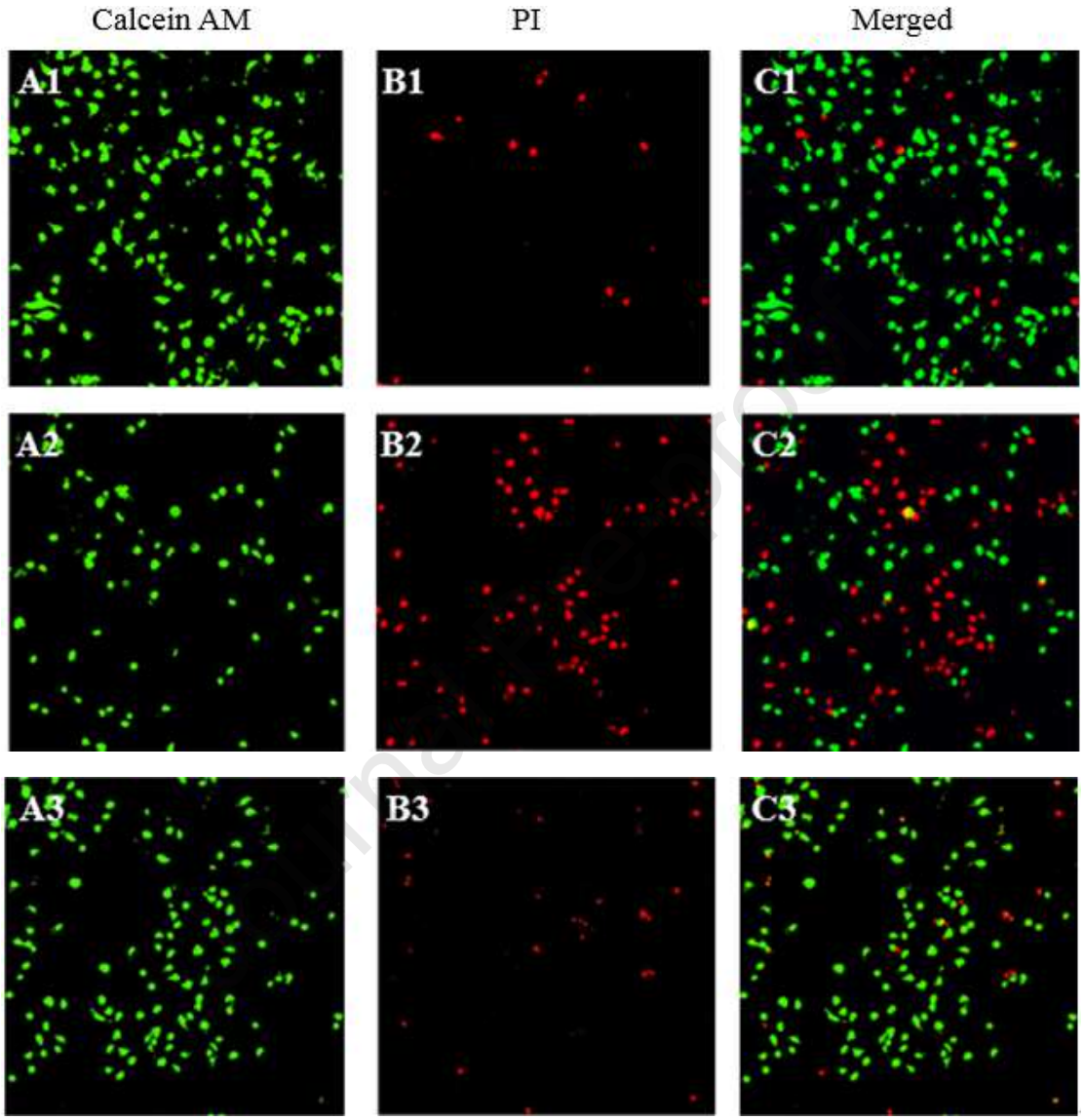

Figure 10. Morphological changes of SH-SY5Y cells induced by H_2O_2. SH-SY5Y cells treated with DMSO (A1-C1) and pre-incubated with **22** (10 μM) (A2-C2) for 6 h at 37 ^{o}C followed with treatment of H_2O_2 (100 μM) for another 24 h. The group treated with H_2O_2 (100 μM) for 24 h was used as positive control (A3-C3). After 24 h co-incubation, the cells were collected and co-stained with calcein AM/PI double staining solution. The results were recorded and analyzed with laser confocal microscope and represented as one of three independent experiments.

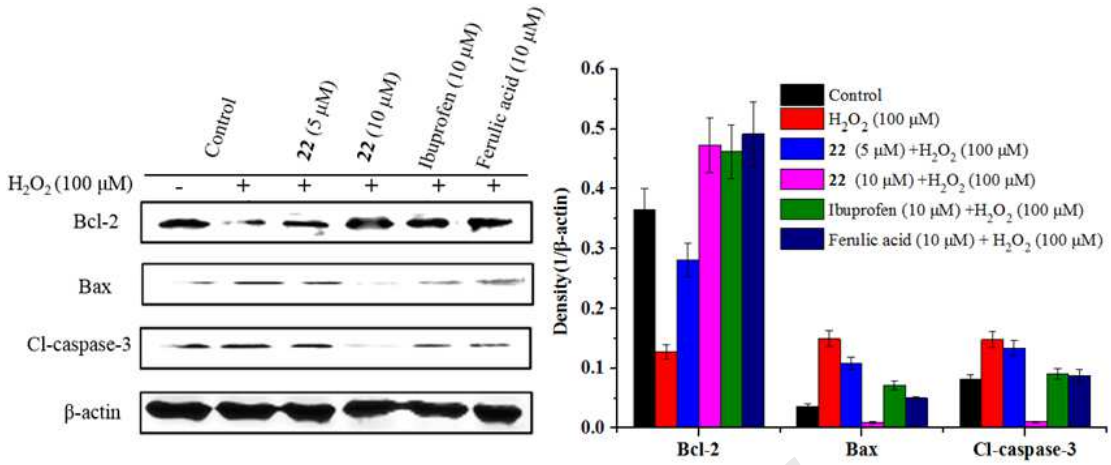

Figure 11. Western blotting analysis of the neuroprotective effects induced by **22**. SH-SY5Y cells were pretreated with DMSO, **22** (5 μM, 10 μM), Ibuprofen (10 μM) and ferulic acid (10 μM) for 6 h before exposure to H_2O_2 (100 μM) for another 24 h. After incubation, total cytosolic protein was collected and subjected to western blotting analysis. Levels of relative proteins were obtained from western blotting and normalized with β-actin. Data were showed as the mean ±SD of three independent experiments.

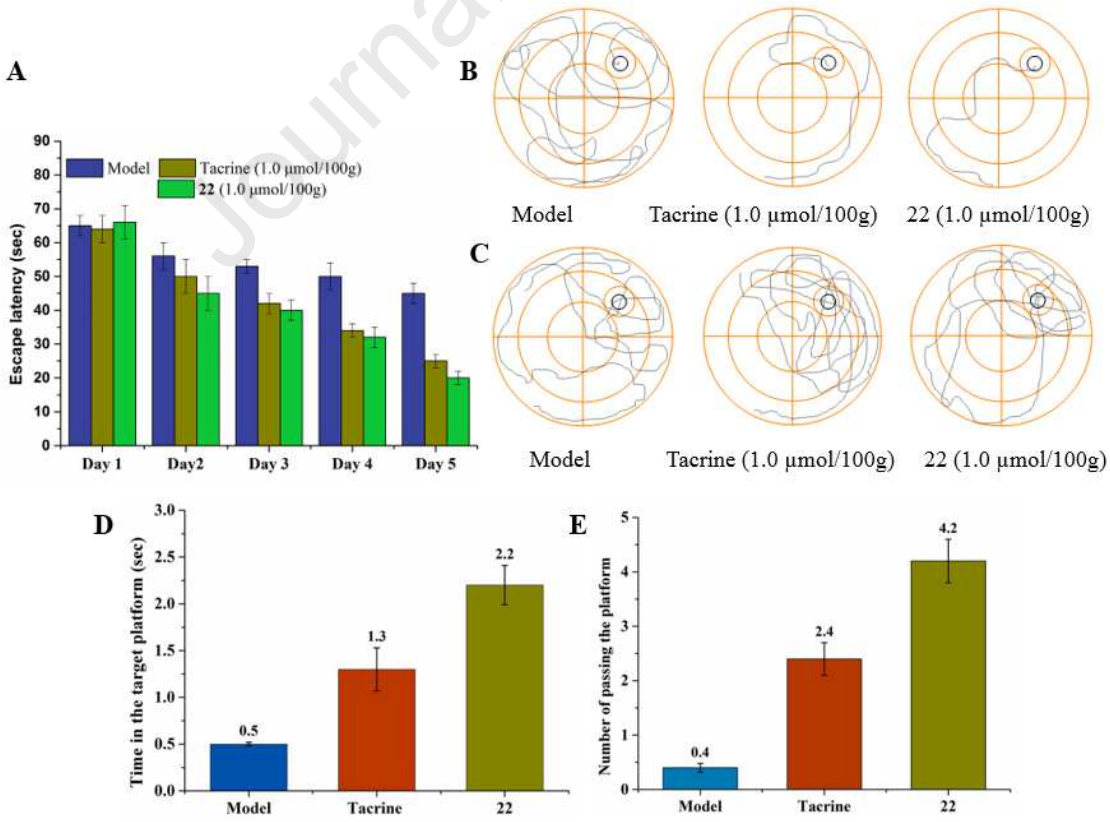

Figure 12. Morris water maze (MWM) assay of therapeutic effects on memory impairment

induced by intracerebroventricular injection with $A\beta_{25-35}$. Total fifteen rats in three independent groups were used for the following cognitive and memory tests after 4 weeks daily intraperitoneal injection with control (normal saline), tacrine (1.0 μmol/100g, 0.2 mg/100g, qd) or **22** (1.0 μmol/100g, 0.9 mg/100g, qd). (A) Memory training in 4 weeks of various samples treatment. (B) The representative tracks during the memory training in day 5. (C) Representative paths in the spatial probe experiments. (D/E) Numbers were obtained upon the virtual platform quadrant. The results were presented as mean ± SD (n =5).

Highlights

► Novel prodrugs releasing ibuprofen and tacrine derivative upon exposure to H_2O_2.

► Good neuroprotective activities against H_2O_2 through mitochondrial apoptosis pathway.

► Efficiently attenuate proinflammatory cytokines (IL-1β, TNF-α) induced by LPS upon H_2O_2-treatment.

► Effectively enhance the ability of learning and memory in Aβ-induced AD model.

Declaration of interests

☒ The authors declare that they have no known competing financial interests or personal relationships that could have appeared to influence the work reported in this paper.

☐The authors declare the following financial interests/personal relationships which may be considered as potential competing interests: